NAVAL POSTGRADUATE SCHOOL

MONTEREY, CALIFORNIA

THESIS

INVESTIGATION OF PANCHROMATIC SATELLITE IMAGERY SENSOR LOW BIAS IN SHADOW METHOD AEROSOL OPTICAL DEPTH RETRIEVAL

by

Brian J. Rivenbark

March 2009

Thesis Advisor: Philip A. Durkee
Second Reader: Kurt E. Nielsen

Approved for public release; distribution is unlimited

THIS PAGE INTENTIONALLY LEFT BLANK

REPORT DOCUMENTATION PAGE		Form Approved OMB No. 0704-0188

1. AGENCY USE ONLY *(Leave blank)*	2. REPORT DATE	3. REPORT TYPE AND DATES COVERED
	March 2009	Master's Thesis

4. TITLE AND SUBTITLE Investigation of Panchromatic Satellite Imagery Sensor Low Bias in Shadow Method Aerosol Optical Depth Retrieval.	5. FUNDING NUMBERS
6. AUTHOR(S) Brian J. Rivenbark	
7. PERFORMING ORGANIZATION NAME(S) AND ADDRESS(ES) Naval Postgraduate School Monterey, CA 93943-5000	8. PERFORMING ORGANIZATION REPORT NUMBER
9. SPONSORING /MONITORING AGENCY NAME(S) AND ADDRESS(ES) N/A	10. SPONSORING/MONITORING AGENCY REPORT NUMBER

11. SUPPLEMENTARY NOTES The views expressed in this thesis are those of the author and do not reflect the official policy or position of the Department of Defense or the U.S. Government.

12a. DISTRIBUTION / AVAILABILITY STATEMENT	12b. DISTRIBUTION CODE
Approved for public release; distribution is unlimited	

13. ABSTRACT (maximum 200 words)

A technique known as the Shadow Method was developed for calculating aerosol optical depths by measuring the radiance difference between shaded and unshaded regions in high-resolution satellite imagery by Vincent (2006). Previous research investigated use of the Shadow Method in regions of dust obscuration using buildings and clouds as shadow generation sources and a variety of background surfaces. A recurring low bias was seen when using the Shadow Method with the QuickBird satellite's panchromatic sensor. QuickBird and WorldView1 commercial imagery was examined using the Shadow Method at several sites co-located with AERONET observations sites. The results show that low bias is not attributed to sensor calibration, processing methods of the imagery, or water vapor content. The most likely source of low bias is the region of interest (ROI) selection geometry within the shadow regions.

14. SUBJECT TERMS	15. NUMBER OF PAGES
Aerosol Optical Depth Retrieval, AOD, High-Resolution Commercial Imagery, QuickBird, WorldView1, Shadow Method, Cloud Shadows.	77
	16. PRICE CODE

17. SECURITY CLASSIFICATION OF REPORT	18. SECURITY CLASSIFICATION OF THIS PAGE	19. SECURITY CLASSIFICATION OF ABSTRACT	20. LIMITATION OF ABSTRACT
Unclassified	Unclassified	Unclassified	UU

NSN 7540-01-280-5500

Standard Form 298 (Rev. 2-89)
Prescribed by ANSI Std. 239-18

THIS PAGE INTENTIONALLY LEFT BLANK

Approved for public release; distribution is unlimited

INVESTIGATION OF PANCHROMATIC SATELLITE IMAGERY SENSOR LOW BIAS IN SHADOW METHOD AEROSOL OPTICAL DEPTH RETRIEVAL

Brian J. Rivenbark
Lieutenant Commander, United States Navy
B.S., United States Naval Academy, 1994

Submitted in partial fulfillment of the
requirements for the degree of

MASTER OF SCIENCE IN METEOROLOGY AND PHYSICAL OCEANOGRAPHY

from the

NAVAL POSTGRADUATE SCHOOL
March 2009

Author: Brian J. Rivenbark

Approved by: Philip A. Durkee
Thesis Advisor

Kurt E. Nielsen
Second Reader

Philip A. Durkee
Chairman, Department of Meteorology

THIS PAGE INTENTIONALLY LEFT BLANK

ABSTRACT

A technique known as the Shadow Method was developed for calculating aerosol optical depths by measuring the radiance difference between shaded and unshaded regions in high-resolution satellite imagery by Vincent (2006). Previous research investigated use of the Shadow Method in regions of dust obscuration using buildings and clouds as shadow generation sources over a variety of background surfaces. A recurring low bias was seen when using the Shadow Method with the QuickBird satellite's panchromatic sensor. QuickBrid and WorldView1 commercial imagery was examined using the Shadow Method at several sites co-located with AERONET observations sites. The results show that low bias is not attributed to sensor calibration, processing methods of the imagery, or water vapor content. The most likely source of low bias is the region of interest (ROI) selection geometry within the shadow regions.

THIS PAGE INTENTIONALLY LEFT BLANK

TABLE OF CONTENTS

LIST OF FIGURES

LIST OF TABLES

THIS PAGE INTENTIONALLY LEFT BLANK

ACKNOWLEDGMENTS

A heartfelt thanks to Professor Phil Durkee for giving me the opportunity to work with him on this research topic. I would also like to thank Professor Richard Olsen, Kurt Nielsen, Mary Jordan, Donna Burych, Bob Creasey and Angela Puetz for assisting and mentoring me through my data collection, data processing and thesis research. Thanks to LCDR Mike Loomis, Capt. Darrin Murphy, and Capt. Kevin Quinn for making the Meteorology Deptartment Remote Sensing Lab an enjoyable place to work. Lastly, thanks to my wife, Maria; daughter, Samantha; and son, Austin, for making our time here in Monterey such a memorable chapter in our lives.

THIS PAGE INTENTIONALLY LEFT BLANK

I. INTRODUCTION

According to DoD Joint Publication 3-59, environmental data is considered intelligence information and is deemed critically important to successful military operations planning (JP 3-59 2008). Atmospheric aerosols are an important component in the characterization of the operational environment for military operations planning. Aerosols can have a significant impact on the transmittance and absorption of electro-optical (EO) energy through the atmosphere. Sources for atmospheric aerosols include blowing dust, fires, sea-spray, volcanic activity and burning of fossil fuels. Most commonly we see the impact in the form of reduced visibility as detected by our eyes in the visible light spectrum. Aerosols may also impact other systems, such as weapons guidance and detection sensors and reconnaissance sensors which utilize energy in the other regions of the EO spectrum.

Measuring atmospheric aerosol is most commonly performed by highly sensitive, *in situ* research instruments resulting in a determination of the aerosol optical depth (AOD) value. While these instruments may be well suited for academic research, they are generally not useful for battlefield measurements. Airborne and space-based remote sensing techniques are much more practical and efficient for the determination of tactically relevant AOD information. Several of these techniques have been developed in recent years with the advent of increasingly advanced satellite and airborne imaging devices. Using remote sensing techniques to measure AOD at the global and regional scale is very useful in earth radiation budget calculations and climate research, but may be too generalized for use with current tactical decision aids in the high-resolution, high-precision environment of the modern battlefield.

One of the most operationally relevant approaches to measuring AOD was developed by Vincent (2006). This technique, known as the Shadow Method, uses high resolution commercial satellite imaging systems to measure radiance values inside and outside of shadows in the scene. With commercial imager resolutions on the order of less than 1 meter, shadows from small features such as buildings can be used to effectively measure the AOD in the region of interest. Follow on research in the last two years has

further refined the use of the Shadow Method. Dombrock (2007) determined that steps in the Shadow Method could be automated for quicker AOD calculations and developed a strategy to best measure the shaded radiance for a given shadow morphology. Evans (2007) compared and evaluated the technique using QuickBird's multi-spectral and panchromatic (PAN) sensor channels for various scene surfaces. Sweat (2008) proved the use of clouds as effective shadow generation sources for the technique using several different satellite platforms and sensors.

A common result from this body of work has been a low-bias in the calculated AOD value compared to *in situ* measured AOD value when using the QuickBird panchromatic (PAN) sensor. This low-bias error was not consistent across all the examined cases in the previous research, and differing theories for this error have been proposed. This thesis will investigate the potential sources for this error by comparing the calculated AOD from both the QuickBird PAN sensor and the new WorldView1 satellite's PAN sensor and evaluating against *in situ* AOD observations at a variety of locations worldwide.

II. BACKGROUND

A. RELATED RESEARCH

The following are short summaries of previously developed techniques for determining overland aerosol optical depth (AOD) using remote sensing systems. According to Vincent (2006), all these methods were subject to three basic problems when measuring AOD over land: background types which saturate certain channels of the sensor, highly variable and complex surfaces which prevent accurate characterization; and large enough number of sensor channels at correct wavelengths to overcome the first two problems.

1. Contrast Reduction Methods

Odell and Weinman (1975) used the adding method to solve the Radiative Transfer Equation (RTE) by developing a contrast modulation function using a relationship between aerosol optical depth and the radiances for two objects with varying albedo. Tanre et al. (1981) used a single scatter approximation and a correction algorithm to determine background influence on reflectance by taking the difference between target and background pixel radiances. Kaufman and Joseph (1982) developed an automated procedure for calculating AOD using imagery features containing large differences in surface albedo. This technique, known as the "two-halves" approach, suffered from high sensitivity to variation in single scatter albedo.

2. Dark Object Method

The Dark Object Method relies on using a low reflectance background, such as dark vegetation or deep water, in order to assume no contribution from surface radiance, leaving any measured path radiance in the area of interest the result of aerosol reflectance. Kaufman and Sendra (1988) created an algorithm for correcting visible and Near Infrared (NIR) imagery based on this principle using regions of dark vegetation. Though effective, this technique is limited to use in regions which contain sufficiently dark surfaces.

A refinement to this method, known as “Deep Blue”, was developed by Hsu et al. (2004). This technique exploits the fact that many regions such as deserts and urban areas have a high surface reflectivity in the red and NIR regions but much lower surface reflectivity in the blue end of the EO spectrum. Using two blue channels in combination, AOD can be estimated providing the surface reflectance is not too great. This method is limited to having a sensor which provides more than one channel in the blue region, such as MODIS or SeaWIFS, as well as assumptions in surface reflectance and aerosol shape.

3. Multi-Angle Method

The multi-angle method for land-based AOD retrievals utilizes the unique capability of multi-view sensors. The Along Track Scanning Radiometer 2 (ATSR-2) investigated by Veefkind et al. (1998) and the Multi-angle Imaging SpectroRadiometer (MISR) investigated by Martonchik et al. (2004) provide multiple views on the target area as the satellite passes overhead. These nearly instantaneous views from different angles allow for an accurate characterization of surface reflectance. Combining this information with modeled aerosol angular scattering properties can provide accurate AOD retrievals. Though effective, this method is limited to the few multi-angle research sensors currently in orbit and can not be relied upon for tactical military support.

B. SHADOW METHOD

1. Introduction

The Shadow Method capitalizes on the very high resolution of today’s commercial satellite imaging systems, specifically the QuickBird and WorldView sensors developed by DigitalGlobe, Inc. Shadows from previously indistinguishable scene detail may now be exploited to calculate AOD without *a prior* knowledge of the aerosol type, or surface reflectance. By measuring the difference in radiance inside and outside of multiple shadow areas, a scene-average AOD can be calculated for the area of interest.

2. Shadow Method Summary

Vincent (2006) developed the Shadow Method based on the principle-of-invariance method of radiative transfer. This method accounts for the radiative effects of

direct transmission, diffuse transmission, and diffuse reflection back to the surface. When combined, these three components result in the top of the atmosphere (TOA) radiance measured by a satellite sensor. The Shadow Method uses the difference in measured radiance from inside and outside a shadow region to solve for the direct transmission component of the total irradiance reaching the satellite. The direct transmission component can then be used to provide optical depth information. The concept behind the Shadow Method is illustrated in Figure 1.

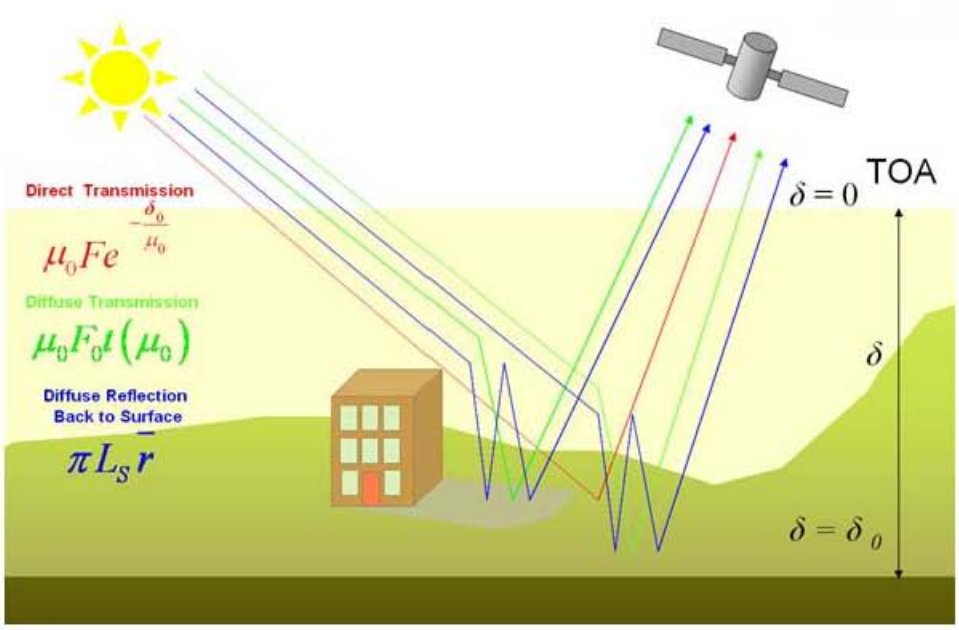

Figure 1. The Shadow Method uses the difference between the radiances within and outside of a shadow area to quantify the direct transmission and total optical depth. (From: Vincent 2006)

3. Governing Equation

The governing equation is derived from the accounting of each component contributing to the top of the atmosphere (TOA) radiance. Vincent (2006) provides a detail account of the derivation and a summary of this derivation follows.

Expressions for the three components of total irradiance as seen in Figure 1 are provided in Equations (1), (2), and (3).

Direct transmission is given as,

$$\mu_0 F_0 e^{-\delta_0/\mu_0}, \tag{1}$$

where μ_0 is cosine of the solar zenith angle, F_0 is the spectral solar radiant flux density (irradiance), and δ_0 is the optical depth of the atmosphere.

Diffuse transmission is given as,

$$\mu_0 F_0 t(\delta_0, \mu_0), \tag{2}$$

where *t* is transmittance.

Diffuse reflection is given as,

$$\pi L_s \bar{r}, \tag{3}$$

where L_s is surface radiance, and $\bar{r}$ is the mean aerosol reflectance.

The total irradiance or flux density is given by,

$$\pi L_s = r_s \left(\mu_0 F_0 e^{-\delta_0/\mu_0} + \mu_0 F_0 t(\delta_0, \mu_0) + \pi L_s \bar{r} \right). \tag{4}$$

where r_s is surface reflectance.

Solving for surface radiance, L_s, gives,

$$L_s = \frac{r_s}{1 - r_s \bar{r}} \frac{\mu_0 F_0}{\pi} \left(e^{-\delta_0/\mu_0} + t(\delta_0, \mu_0) \right). \tag{5}$$

This form represents surface radiance measured at the surface. Viewed from the satellite as TOA radiance requires interaction with the atmosphere (attenuation) given by,

$$L_s = \left[\frac{r_s}{1 - r_s \bar{r}} \frac{\mu_0 F_0}{\pi} \left(e^{-\delta_0/\mu_0} + t(\delta_0, \mu_0) \right) \right] e^{(-\delta_0/\mu)}. \tag{6}$$

This form also represents the unshaded radiance component for the region of interest. The shaded component of the region of interest will be essentially the same, but without the direct transmission contribution (inside the shadow) represented by,

$$L_s^{\,shaded} = \left[\frac{r_s}{1 - r_s \bar{r}} \frac{\mu_0 F_0}{\pi} t(\delta_0, \mu_0) \right] e^{(-\delta_0 / \mu)}. \quad (7)$$

If a region of interest can be selected such that the shaded and unshaded areas provide a homogenous surface reflectance, then the radiance difference, $L_{d,}$ between these areas can be shown as,

$$L_s^{\,unshaded} - L_s^{\,shaded} = L_d = \frac{r_s}{1 - r_s \bar{r}} \frac{\mu_0 F_0}{\pi} e^{-\delta_0 \left(\frac{1}{\mu_0} + \frac{1}{\mu} \right)}. \quad (8)$$

Solving this form for optical depth, δ_0, gives the governing equation for total optical depth (TOD):

$$\delta_0 = \left(\frac{\mu_0 \mu}{\mu + \mu_0} \right) \ln \left[\left(\frac{r_s}{1 - r_s \bar{r}} \right) \left(\frac{\mu_0 F_0}{\pi L_d} \right) \right]. \quad (10)$$

Equation (10) is now used to calculate TOD given the satellite and solar geometry, spectral solar radiance for the sensor channel used and the difference in measured radiance.

4. Optical Depth Due to Molecular Rayleigh Scattering

Vincent (2006) uses the molecular Rayleigh optical depth contribution based on wavelength, pressure, and height from the relationship developed by Russel et al. (1993):

$$\delta_R(\lambda) = \left(0.00864 + 6.5 \times 10^{-6} H \right) \lambda^{-b(\lambda)} \left(p / p_0 \right), \quad (11)$$

$$b(\lambda) = 3.916 + 0.074\lambda + 0.050 / \lambda, \quad (12)$$

where λ is the wavelength (in microns), H is the height above sea level of the radiometer (kilometers), p is the atmospheric pressure at the altitude of the radiometer (hPa), and p_0 is the sea level reference pressure, taken as 1013.24 hPa. Table 1 provides the molecular Rayleigh optical depth calculated for both QuickBird and WorldView1 PAN channels using the center effective wavelength (CEW), a radiometer height of zero (km), and an atmospheric pressure at the radiometer of 1013.25 hPa.

Table 1. Molecular Rayleigh optical depths for the QuickBird and WorldView1 channels, based on equations given by Russel et al. (1993) assuming radiometer height of zero km and atm pressure of 1013.25 hPa.

Channel	Center Effective Wavelength (μm)	Molecular Rayleigh Optical Depth
QB Blue	0.482	0.17
QB Green	0.556	0.092
QB Red	0.658	0.047
QB Near_Infrared	0.816	0.019
QB Panchromatic	0.673	0.043
WV1 Panchromatic	0.666	0.045

As outlined in Vincent's theoretical development of the Shadow Method, the molecular Rayleigh scattering effects are not utilized in the initial determination of mean aerosol reflectance, but are instead used to adjust the final total optical depth calculation. One artifact of this method is seen for very low aerosol optical depth retrievals, where the subtraction of the Rayleigh optical depth may result in negative AOD values. Consequently, this is one of the limiting factors leading to a minimum resolvable AOD of 0.1 when using the Shadow Method (Vincent 2006).

5. Using the Governing Equation

Most of the terms in Eq. (10) are determined by the image scene. Solar and sensor geometry are provided in the image metadata while surface reflectance and radiance difference are derived from measured radiance in the scene. Solar irradiance is a constant for the sensor channel being used. The mean aerosol reflectance is the only term estimated by the user through selection of the aerosol phase function and single scatter albedo. Vincent (2006) provides a sensitivity study for both phase function and single scatter albedo showing that AOD values are not highly dependent on these terms. Vincent also describes his iterative method for solving total optical depth (TOD) based on the initial assumption that aerosol reflectance is much smaller than surface reflectance. The TOD is adjusted for molecular Rayleigh scattering as described in the previous section. The resulting value is the calculated aerosol optical depth (AOD).

C. THE PANCHROMATIC LOW BIAS PROBLEM

Vincent (2006) found a low bias trend in his results when comparing the QuickBird panchromatic channel calculated AOD results with the ground truth AERONET AOD values in several of his case studies. The low bias also appeared in some of these cases for the red and near infrared channels, but to a lesser extent. A low bias was also seen in AOD values resulting from research performed by Evans (2007). However, the low bias was seen in both the multispectral and panchromatic QuickBird channels for Evan's image case study. Figure 2 provides examples of the low bias seen in several image case studies.

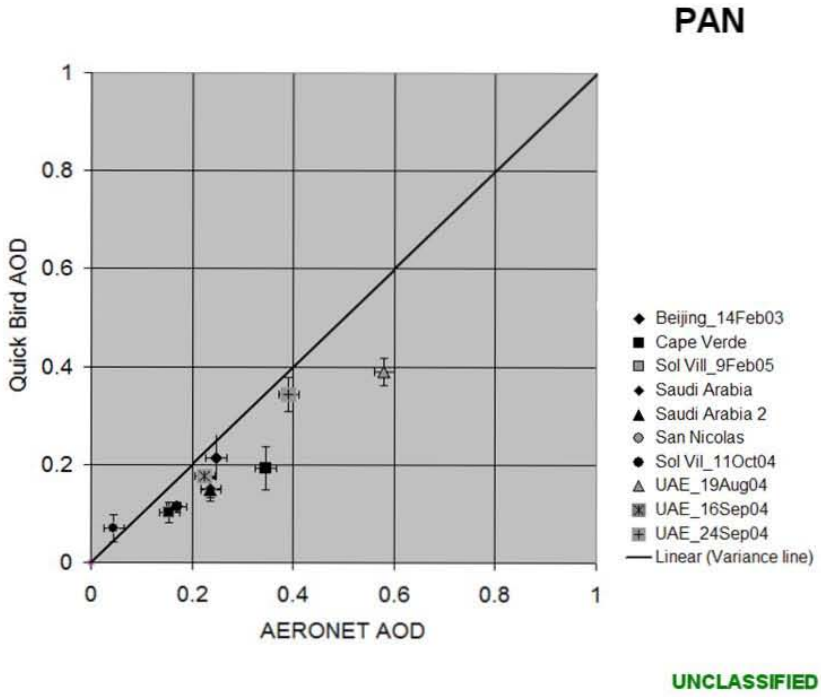

Figure 2. The graphic shows examples of the panchromatic AOD retrieval low bias for several case studies in various locations worldwide. (After: Durkee 2008)

Various explanations of the root cause or contributing causes of this low bias signal have been suggested. These theories and examination methods will be discussed in detail in later chapters. The goal of this research effort is to investigate these potential causes and to identify the source of this error as well as determine the best course of action for accounting for and reducing the effects of this low bias error.

D. THE PANCHROMATIC LOW BIAS INVESTIGATION

The goal of this study was to determine the cause of the low bias in the Shadow Method AOD retrievals using QuickBird panchromatic imaging sensor. If a definite cause could not be identified, verified contributing factors could be eliminated. Vincent (2006) proposed the initial hypothesis for the panchromatic low bias was a result of gaseous absorption due to water vapor. The presence of water vapor would reduce transmittance within the panchromatic channel, decreasing satellite-observed radiance, and reducing the mean retrieved AOD values. Vincent's efforts to account for gaseous absorption due to water vapor did raise mean retrieved AOD values slightly in the three image cases he examined, but did not account for the majority of the low bias signal.

Other hypotheses included: 1) errors in the image processing which failed to account for varying Time Delay Integration and absolute calibration factors for individual images; 2) potential radiometric calibration error in the QuickBird panchromatic sensor itself (originally proposed by Martin (2004); and 3) a systematic error in sampling the higher resolution shadow features in the panchromatic imagery.

Several avenues were proposed to investigate these hypotheses. One approach involved the re-investigation of previously studied cases in which large amplitude low bias was observed. The calibration and water vapor theories would be tested by obtaining near simultaneous collections of both QuickBird and WorldView1 imagery with *in-situ* AOD observations as ground truth. The image pairs would be used to compare AOD retrievals from both sensors and determine if sensor calibration contributed to the low bias. Water vapor observations would also be collected to correlate atmospheric column water vapor and AOD low bias.

III. METHODOLOGY

A. OVERVIEW

As originally stated by Vincent (2006), the shadow-based AOD retrieval method is intended for use with high-spatial resolution (<5 m) commercial satellite imagery with no *a prior* knowledge of surface reflectance or mean aerosol reflectance. Satellite imagery and meta data is pre-processed to orthorectify and calibrate the image. The image is manually analyzed for appropriate shadow regions using the Environment for Visualizing Images (ENVI) version 4.5 visualization software package. Regions of interest (ROI) are selected using the ENVI software and specialized code written in the Interactive Data Language (IDL) version 7.0 is used to extract radiance values from the ROIs and calculate AOD.

B. SATELLITE IMAGERY

1. Imagery Orthorectification

The same orthorectification technique used by Vincent (2006) was used in this study. ENVI 4.5 was selected to use the built-in orthorectification capability for both QuickBird and WorldView1. ENVI 4.5 is the first version to add the capability for reading in WorldView1 metadata and offer this orthorectification feature. ENVI automatically reads in the rational polynomial coefficient and the fixed height information from the imagery metadata, calculates the corrections for each pixel and writes out the new orthorectified image file.

2. Imagery Calibration

Both imagery sets were calibrated for top of the atmosphere radiance values. The BandMath tool in ENVI 4.5 was used to apply the calibration expression below.

$$L_\lambda = \text{ImageDN}_\lambda * \text{abscalfactor}_\lambda / \text{effective bandwidth}_\lambda$$

L_λ is the top of the atmosphere radiance value for the spectral band λ in units of watts per meter squared per nanometer per steradian ($W\ m^{-2}\ nm^{-1}\ sr^{-1}$). ImageDN is the

brightness value measured by the sensor and effective bandwidth represents the spectral band of interest. The absolute calibration factor is based on the Time Delay Integration (TDI) value. The TDI process allows a moving object (such as a satellite) to capture blur-free images as it passes a scene of interest. TDI values are adjustable for both the QB and WV1 PAN sensors, depending on season and latitude, in order to allow the imaging sensor to obtain the best resolution possible. According to Krause (2008), summer image collection missions typically use TDI values of 13 for QB and 16 for WV1, while these values may be increased to 18 for QB and 32 for WV1 during winter or high latitude collection operations. Table 2 lists a sample of the TDI and absolute calibrations factors used for the panchromatic sensor calibration expressions in this study.

Table 2. TDI values, Calibration Coefficients and Bandwidth for QuickBird and WorldView1 Panchromatic channels. (DigitalGlobe 2008)

Band	TDI Level	Absolute Calibration Factor	Bandwidth (μm)
QB PAN	13	6.447600e-02	.398
QB PAN	10	8.381880e-02	.398
WV1 PAN	16	6.243908e-02	.372

3. ROI Sampling

Regions of Interest (ROI) must be generated within the ENVI interface for each shaded / unshaded area pair. This ROI contains pixel samples from within both the shaded and unshaded area over a homogeneous surface. Each ROI is analyzed by ENVI's ROI Statistics function, which generates minimum, mean, maximum and standard deviation values for each ROI.

Previous work on the shadow technique by Evans (2007) and Dombrock (2007) determined that using mean radiance value sampling within the shaded regions, instead of minimum or mode value sampling, improved AOD calculation results for the multispectral and panchromatic QuickBird channels when compared to ground truth observations.

Research by Dombrock (2007) also suggested that care must be taken in selecting ROI pairs due to the interaction of surrounding shadow generators and the color of the primary shadow generator on the measured radiance values. Additionally, the proximity of pixels inside the shaded region to the shadow edge affects the measured radiance values due to blockage of the celestial dome and diffuse sky radiance in those areas nearest to the shadow generator base and furthest away from the shadow edge.

With these considerations in mind, ROIs were selected which had a minimum proximity to other large shadow generators and a homogenous surface for both shaded and unshaded regions. The shaded regions were selected as far away from the shadow generator as possible, without getting shadow edge influence, in order to reduce celestial dome blocking by the generator. In some cases, more than one ROI pair was selected to determine if AOD variation would occur based on ROI geometry. All ROI data files and locations were saved for use in future research.

4. AOD Extraction

AOD retrievals were calculated using code originally written by Vincent (2006), modified by Dombrock (2007), and further edited in the course of study. The AOD extraction and calculation code is written in the Interactive Data Language (IDL), and most recently compiled in IDL version 7.02. The code also contains components which use specialized ENVI function calls, requiring both the ENVI and IDL environments to be active in order for the code to compile and run properly.

Previous research compared AOD results using minimum, maximum, mean and mode radiance values for ROI data extractions. Dombrock (2007) concluded that the mean radiance values were most consistent and representative for calculating AOD. Although ROIs are chosen with as near to homogeneous surfaces as possible, variation in the pixel radiance does occur and can provide erroneous results when only minimum or maximum radiance values are used. Mean radiance values were used in the AOD extraction code for this study.

THIS PAGE INTENTIONALLY LEFT BLANK

IV. DATA

A. SATELLITE IMAGERY

Commercial satellite imagery from the QuickBird and WorldView1 satellites, both launched and operated by Digital Globe, Inc., were used in this study. All satellite images and meta-data files were delivered via mail on DVD in the standard .NTF file format.

1. QuickBird

The QuickBird satellite, placed into service in October 2001, provides high resolution imagery products for both multispectral and panchromatic channels. The channel resolutions achieved at near-nadir views are 0.60 m for the panchromatic (445-520 nm) and 2.4 m for the multispectral channels (blue (450-520 nm), green (520-600 nm), red (630-690 nm) and near-infrared (760-900 nm) with a dynamic range of 11-bits per pixel. The high resolution imagery from QuickBird reveals shadow features previously unavailable in commercial imagery and these shadows can be exploited using the Shadow Method. Table 3 shows the minimum, maximum, and center effective wavelengths along with the solar spectral irradiance for each channel.

Table 3. QuickBird and WorldView1 minimum, maximum and center effective wavelengths (After: DigitalGlobe (2007)) and band specific spectral solar irradiance based on Wehrli (1985) spectral solar irradiance values.

QB Channel	Minimum Wavelength (nm)	Maximum Wavelength (nm)	Center Effective Wavelength (nm)	Spectral Solar Irradiance (Wm^{-2} nm^{-1})
QB Ch 1-Blue	450	520	482	1973
QB Ch 2-Green	520	600	556	1854
QB Ch 3-Red	630	690	658	1570
QB Ch 4-NIR	760	900	816	1095
QB PAN	445	900	673	1506
WV1 PAN	400	900	666	1493

Orbital characteristics for QuickBird include 450 km altitude, 98 degree sun-synchronous inclination and a period of 93.4 minutes. The local equator crossing time of approximately 10:30 AM provides excellent opportunity for shadow exploitation and a target revisit interval of around 3-7 days depending on target latitude. Scene dimensions for most images are approximately 16.5 km square, with some collections taken as strips of 16.5 km by 165 km long. The imaging sensors are capable of both in-track and cross-track viewing angles up to 30 degree off-nadir and can collect up to 57 images (128 GB) per orbit (DigitalGlobe 2007). The QuickBird panchromatic sensor is also capable of varying the Time Delay Integration (TDI) at five selectable levels ranging from 10 to 32 (Krause 2003). Variations in TDI help account for high latitude and winter season collections where lower solar radiance conditions may exist.

2. WorldView1

WorldView1 was placed into operation in September 2007 and is considered the most agile satellite ever flown commercially. This satellite carries only a panchromatic sensor, but is capable of collecting over 290,000 square miles (750,000 km^2) of imagery per day. The sensor has a resolution of 0.5 m at nadir and 0.59 m at 25 degrees off-nadir with a dynamic range of 11-bits per pixel. Table 3 shows the minimum, maximum, and center effective wavelengths along with the solar spectral irradiance for the panchromatic channel. Orbital characteristics for WorldView1 include 496 km altitude, sun-synchronous orbit with a period of 94.6 minutes. The local equator crossing time is also 10:30 AM and the increased retargeting agility provides a target revisit interval of 1.7 – 4.6 days depending on latitude. WorldView1 is capable of several collection scenarios, ranging from individual 17.6 km square images, long strip images 17.6 km wide by 330km long, to stereo collect areas 30km wide by 110 km long. Max viewing angle is 45 degree off nadir and can collect up to 331 GB per orbit (more than twice that of QuickBird). WorldView1 is also capable of varying the TDI at six selectable levels from 8 to 64 (DigitalGlobe 2007).

B. AERONET OBSERVATIONAL DATA

The Aerosol Robotic Network (AERONET) is a federation of optical ground-based remote sensing aerosol networks established by NASA and Labratoire d'Optique Atmospheric (LOA)-PHOTONS of France. The program provides long-term, continuous and readily accessible databases of aerosol optical, microphysical and radiative properties for aerosol research (GSFC 2008). AERONET stations are located throughout the world with some stations operating continuously for many years and others with fairly short periods of record depending on the site. AERONET stations with available periods of record since the Sep 2007 launch of the WorldView1 satellite were used in the comparison case studies for the two panchromatic sensors.

AERONET stations provide optical depths for several standard wavelengths and atmospheric column water vapor content at three levels of data quality control. Level 1.0 is raw data from the sensor, Level 1.5 is automatically corrected for presence of clouds, and Level 2.0 is corrected for clouds and reviewed for quality control. If available, Level 2.0 was used throughout this effort, otherwise the AERONET data level is annotated for each case study. The standard AERONET channels are listed in Table 4.

Table 4. Standard AERONET Channels and bandwidths (GSFC 2008). (From: Vincent 2006)

Standard AERONET Wavelengths (nm)	**Bandwidth (nm)**
340	2
380	4
440	10
500	10
675	10
870	10
940	10
1020	10

The standard channels are not always available at all stations, with some stations having as few as four channels available. AERONET channels do not exactly match the

center effective wavelengths for the QuickBird or WorldView1 channels. The same comparison technique used by Vincent (2006) was applied in this study. Band-averaged aerosol optical depths for the satellite sensor channels were determined using exponential or power best-fit curves to approximate the spectral distribution of AERONET values and then averaged over the sensor channel bandwidth using the spectral response function of that channel (Vincent 2006). The calculated aerosol optical depth is used as ground truth for the QuickBird and WorldView1 channels with an uncertainty of ± 0.02 (Holben 1998).

V. PREVIOUS CASE STUDY REVIEW AND INVESTIGATION

This portion of the study reviews imagery and observations from previous research conducted by Vincent (2006) and Evans (2007) on the Shadow Method.

A. TIME DELAY INTEGRATION AND ABSOLUTE CALIBRATION

The Time Delay Integral (TDI) variability and the consequent variability in the absolute calibration factor for the QuickBird panchromatic channel represents a potential cause of AOD retrieval error. If the wrong absolute calibration factor was applied when converting to top of the atmosphere radiance, the result could be either artificially high or low radiance values for the entire scene. Previous research using the QuickBird PAN channels made no mention of accounting for variation in the TDI and resulting absolute calibration factor when converting the imagery files to top of the atmosphere radiance. Previous cases with the largest low bias error, seen in Figure 3 were reviewed. Only one image case was found to have a TDI / absolute calibration factor that varied from the normal summertime, mid-latitude collection setting of TDI = 13 and abs. cal. factor = 6.447600e-02.

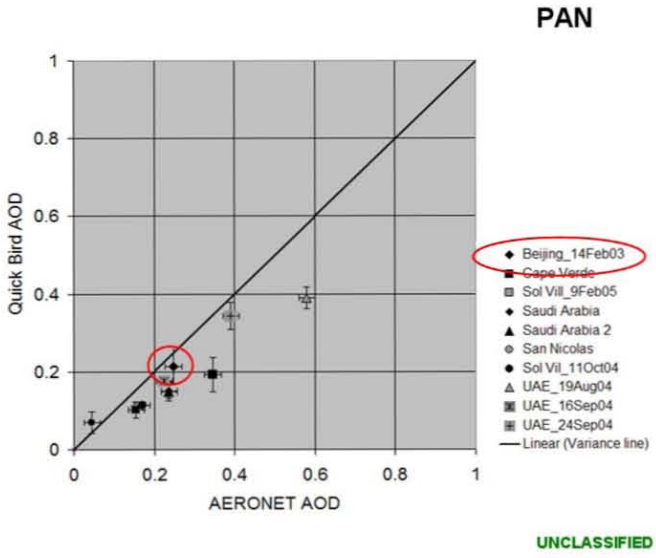

Figure 3. Feb. 14, 2003 Beijing, China image with winter time collection TDI / absolute calibration factor. Based on small magnitude of low bias, TDI / absolute calibration factor variation is not a likely source of error. (After: Durkee 2008)

A TDI level of 18 and abs. cal. factor of 4.656600e-02 was listed in the metadata file for this image collected over Beijing, China on February 14, 2003. These values were consistent with the DigitalGlobe operational guidance for winter time collection as provided by Krause (2008). This case had relatively small low bias as compared with the other cases, and was the only image that varied from the normal TDI/absolute calibration factor settings. Based on this finding, it was determined that the overall low bias error is not likely due to processing error in the image calibration.

B. WATER VAPOR IMPACTS

Five previous cases with low bias error, seen in Figure 4 were reviewed for possible impacts from water vapor. Figures 5 to 9 show the atmospheric water vapor content (cm) as measured by AERONET sensors nearest the image collection time at five case study locations initially investigated by Vincent (2006) and Evans (2007).

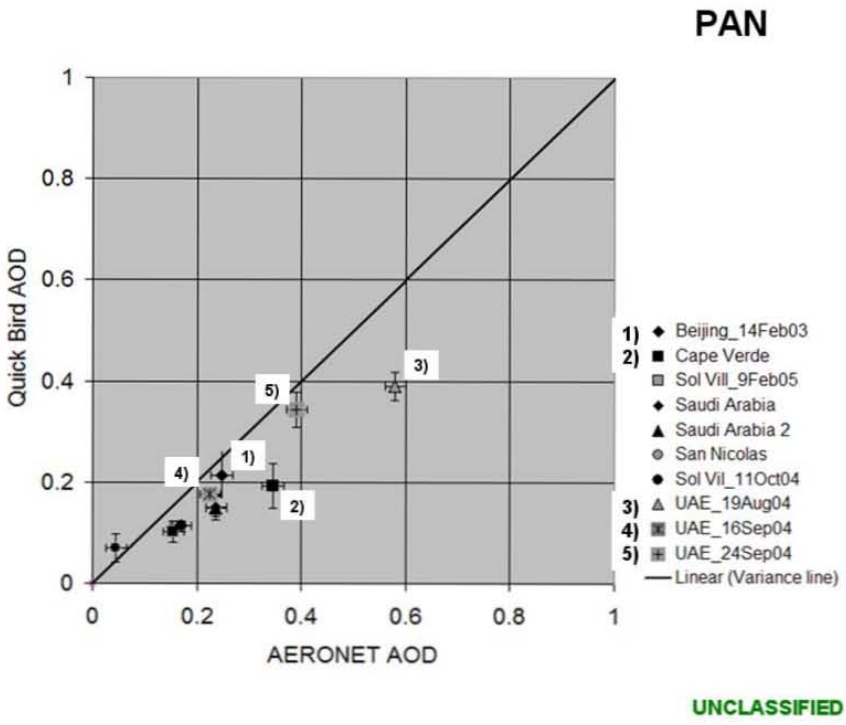

Figure 4. Image cases identified for water vapor investigation. (After: Durkee 2008)

1) Beijing, China – 14 Feb 2003

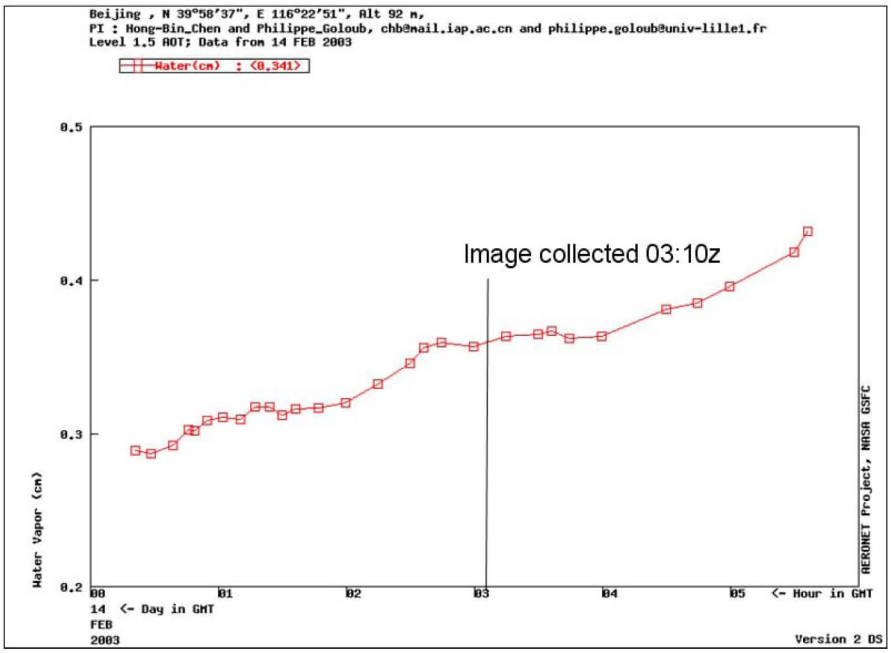

Figure 5. Water vapor content (0.35 cm) for case 1 collected over Beijing on Feb 14, 2003, measured by AERONET.

2) Cape Verde – 26 May 2003

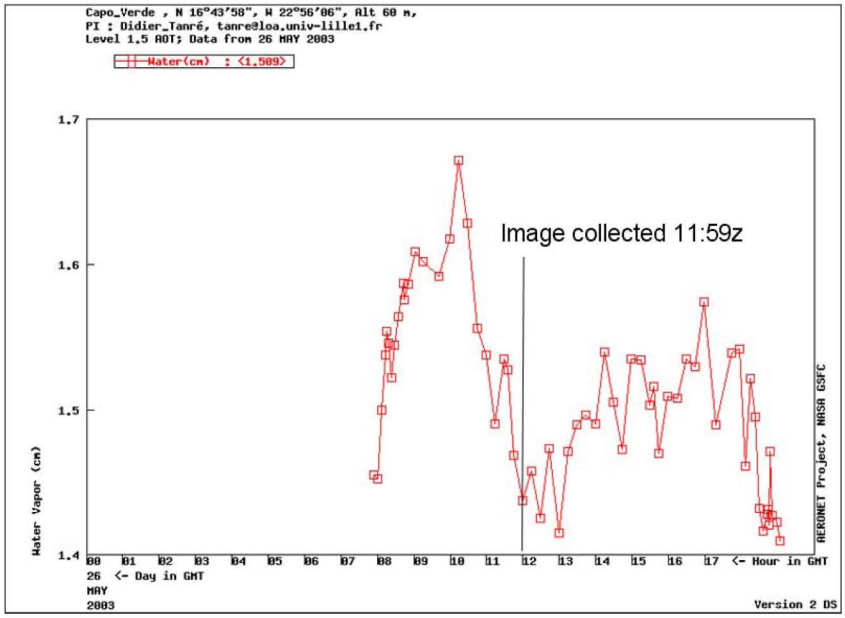

Figure 6. Water vapor content (1.45 cm) for case 2 collected over Cape Verde on May 26, 2003, measured by AERONET.

3) MAARCO station, UAE – 19 Aug 2004

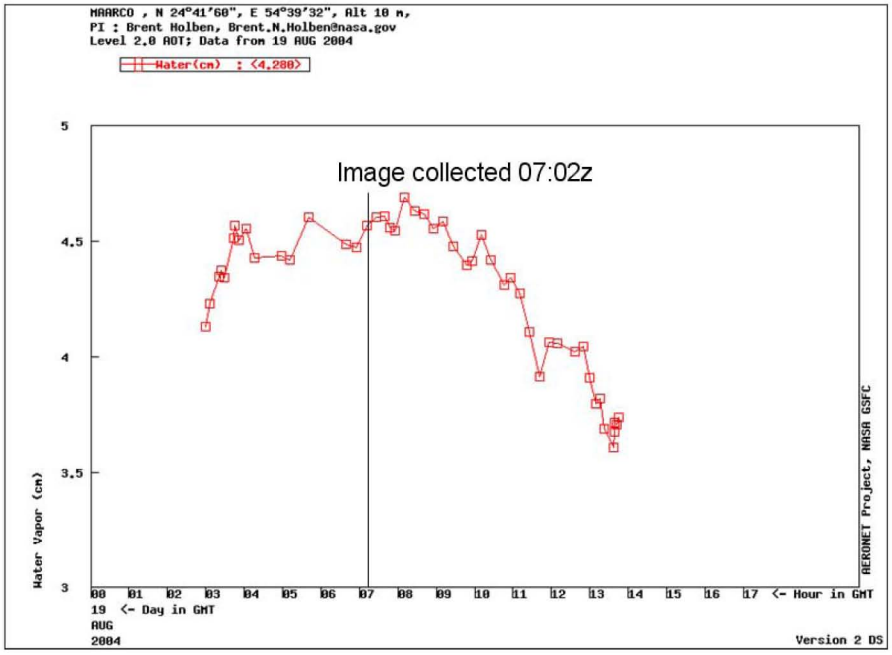

Figure 7. Water vapor content (4.5 cm) for case 3 collected over MAARCO station, UAE on Aug 19, 2004, as measured by AERONET.

4) MAARCO station, UAE – 16 Sep 2004

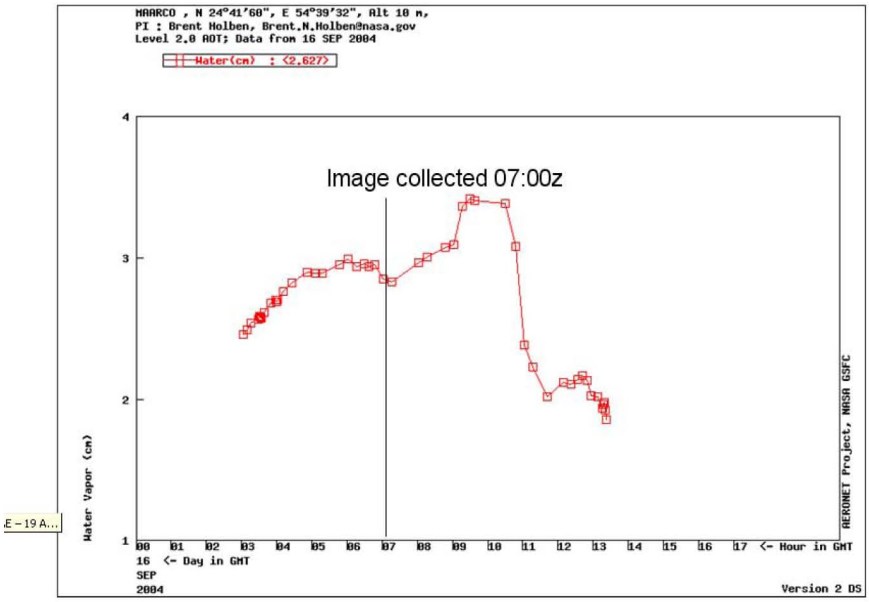

Figure 8. Water vapor content (2.8 cm) for case 4 collected over MAARCO station, UAE on Sep 16, 2004, as measured by AERONET.

5) MAARCO station, UAE – 24 Sep 2004

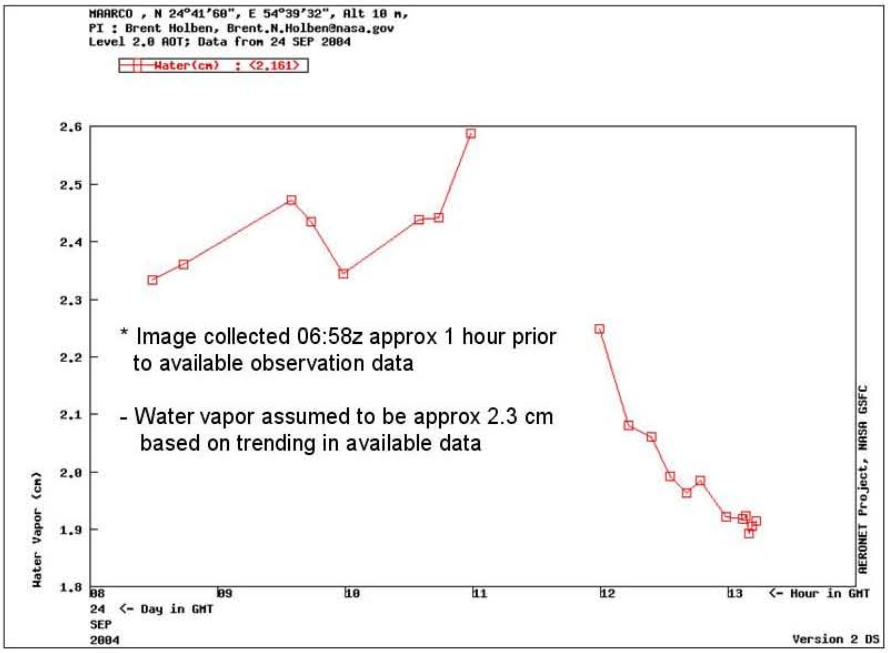

Figure 9. Water vapor content (cm) for case 5 collected over MAARCO station, UAE on Sep 24, 2004, as measured by AERONET. Water vapor estimate is 2.3 cm at time of image collection based on data trend.

Figure 5 shows that water vapor content is about 0.35 cm in the Beijing image (case 1). Case 1 corresponds with a low bias amplitude of about 0.02 seen in Figure 4. The Cape Verde image (case 2) in Figure 6 shows relatively low water vapor content of approximately 1.4 cm. Case 2 has a large low bias amplitude of approximately 0.2. Figure 7 shows relatively high water vapor content of 4.5 cm in the 19 Aug 04 UAE image (case 3). Case 3 also corresponds to a large low bias amplitude of about 0.2. The water vapor content for the UAE images of Sep 04 are shown in Figure 8 (case 4) and Figure 9 (case 5). Case 4 has water vapor of 2.8 cm and a low bias amplitude of about 0.03. Case 5 has water vapor content of 2.3 cm and low bias amplitude of about 0.02. Table 5 summarizes the water vapor and low bias amplitude data.

Table 5. Water vapor content (cm) and low bias amplitude for each image case.

Image Case	Water Vapor Content (cm)	Low Bias Amplitude
1) Beijing -14 Feb 03	0.35	0.02
2) Cape Verde - 26 May 03	1.4	0.2
3) UAE - 19 Aug 04	4.5	0.2
4) UAE - 16 Sep 04	2.8	0.03
5) UAE - 24 Sep 04	2.3	0.02

If water vapor had a consistent influence on the low bias signal, one would expect an approximately linear relationship between water vapor content and the low bias amplitude. Figure 10 shows the plot of water vapor content verses the low bias amplitude. The data does not appear to be linear with a correlation coefficient (R^2) of only 0.17. The image cases and corresponding water vapor data lead to a conclusion that water vapor content does not have a linear influence on the low bias signal.

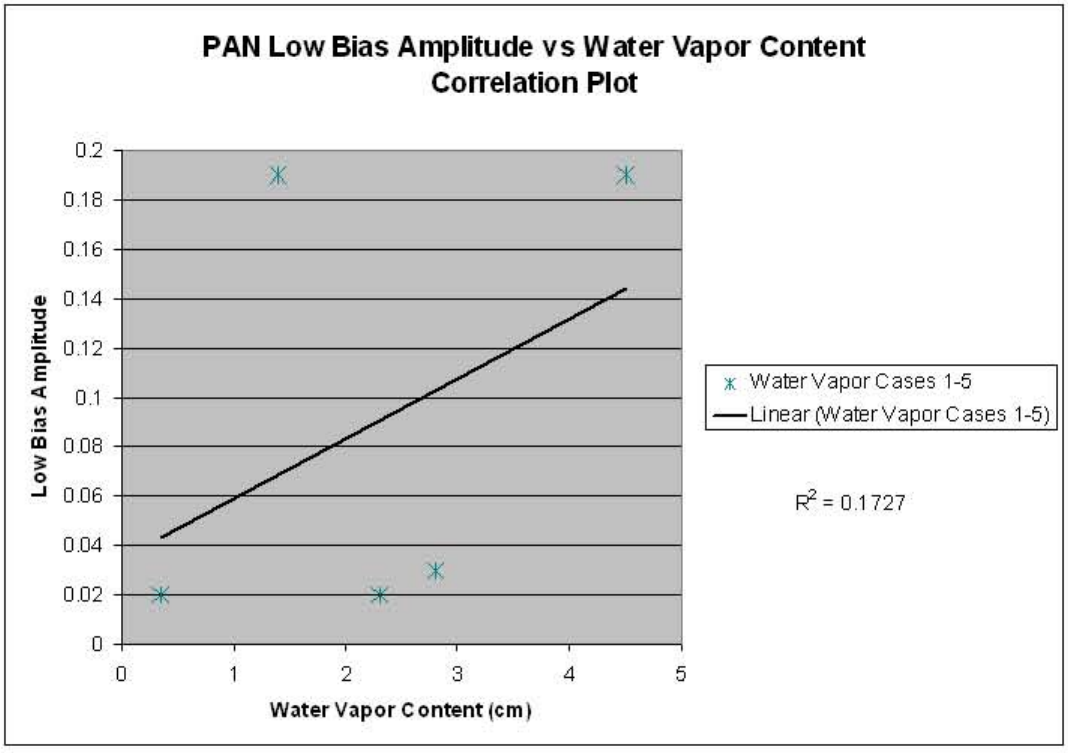

Figure 10. Correlation plot of water vapor (cm) vs low bias amplitude for selected image cases 1 - 5.

C. ROI SELECTION IMPACTS

1. Previous Research

Dombrock (2007) performed a detailed study on the geomorphic influence on radiances inside a shadow region. One of his findings indicated that radiance values inside a shadow region very near the base of the shadow generator will be lower than the radiance values nearer the outer edges due to the blocking out of a portion of the sky by the shadow generator. By blocking out a portion of the sky, or celestial dome, reflected radiance from the atmosphere is reduced into the shadow region, lowering the radiance value and consequently lowering the retrieved AOD value. Dombrock recommended that only the outer 50% of a shadow region should be used as the shaded portion of the ROI pair in performing AOD retrievals to reduce the effect of celestial dome blocking. One possible source of low bias error may be due to this effect on selected ROIs.

Evans (2007) found a significant low bias across all QuickBird channels in his investigation of urban scene AOD retrievals using an image over Beijing, China on September 13, 2003. Evans compared AOD retrievals from a variety of surface types and shadow geometries. The low bias amplitude varied with surface type and channel. Table 6 provides his integrated AERONET AOD ground truths values results, and image retrieved AOD values. Figure 11 shows a comparison of all QuickBird channel results across all surface types and shadow lengths.

Table 6. AERONET integrated AOD. Derived AERONET AOD values matching QuickBird channels and spectral response. (From: Evans 2007)

Channel	**Blue**	**Green**	**Red**	**NIR**	**PAN**
Band (μm)	445-.520	.520-.605	.635-.690	.760-.900	.445-.900
AERONET AOD	0.8860	0.7154	0.5659	0.4097	0.5577
Mean AOD Retrieval	0.79	0.52	0.29	0.22	0.30
Standard Deviation	0.32	0.14	0.09	0.04	0.05

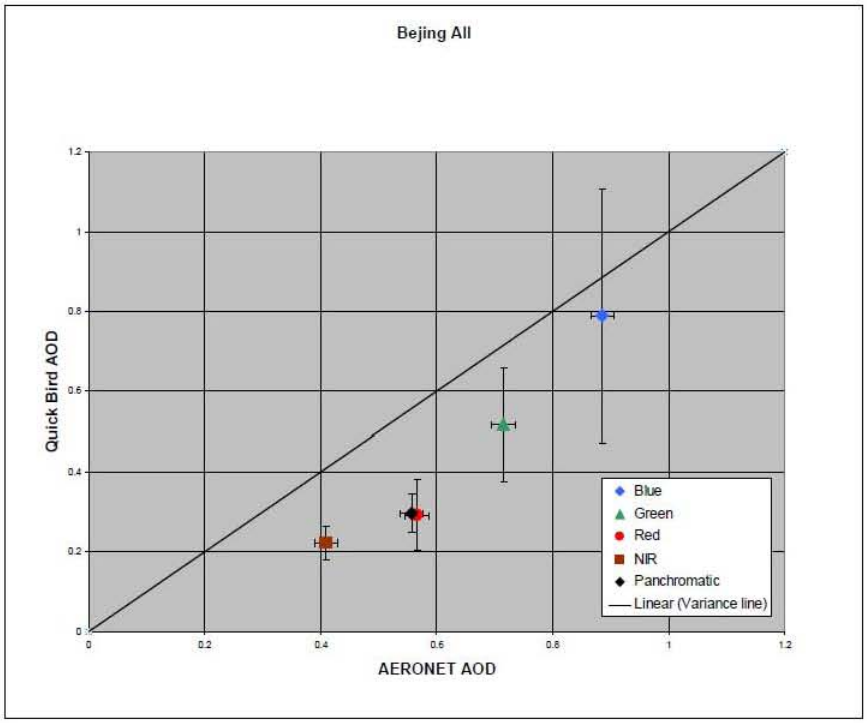

Figure 11. Comparison of QuickBird Shadow Method derived AOD with AERONET derived AOD for ROIs of all surface types and all shadow lengths. Vertical error bars indicated Shadow Method AOD standard deviation while the horizontal error bars indicate uncertainty of the AERONET data. (From: Evans 2007)

Vincent (2006) found a significant low bias primarily in the panchromatic channel, and occasionally in the red or near-infrared channels, depending on the surface type. One possible reason for the consistently low AOD retrievals across all channels in Evans' study is the celestial blocking influence on the urban ROI selection. The September 13, 2003, QuickBird image of Beijing was re-examined and a new set of ROI was generated in an attempt to avoid celestial blocking effects from large shadow generators.

2. Beijing, China, September 13, 2003, QuickBird Re-Investigation

For the purposes of this study, only the panchromatic channel was re-examined. ROIs were selected for shadow regions cast by long thin shadow generators such as towers, smoke stacks, and buildings. When using building shadows, only the outermost 25-30% of the shaded region was used while ensuring the surface regions were homogenous. Twenty-three ROIs were selected across the scene for a variety of surface

backgrounds. Mean AOD retrieval values ranged from 0.346 to 0.605 with a mean value of 0.44. This new mean AOD value is 0.14 greater than that found by Evans and reduces his panchromatic channel low bias by approximately 50%. These results clearly show that careful ROI selection can make a large difference in AOD retrieval accuracy. Figure 12 shows the mean panchromatic AOD retrieval for twenty-three ROIs generated in the re-investigation and Evans' original mean panchromatic AOD.

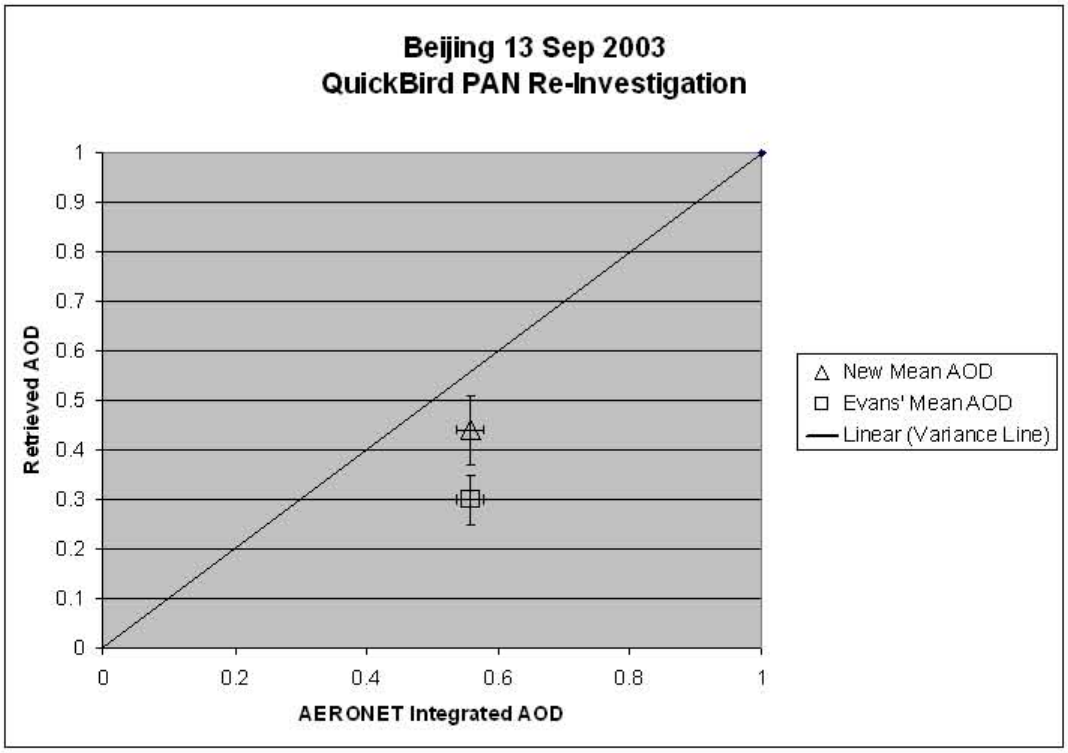

Figure 12. Shadow Method AOD retrievals from the September 13, 2003, Beijing, China image compared with the integrated AOD derived from AERONET. Vertical bars represent AOD retrieval standard deviation and horizontal bars represent AERONET uncertainty.

AOD retrievals were also found to vary within the same shadow, depending on proximity to the shadow generator, further supporting Dombrock's theory on celestial blocking. Two examples of this variation in AOD within the same shadow are provided in Figures 13 and 14. ROIs chosen closer to the shadow generator resulted in lower AOD values.

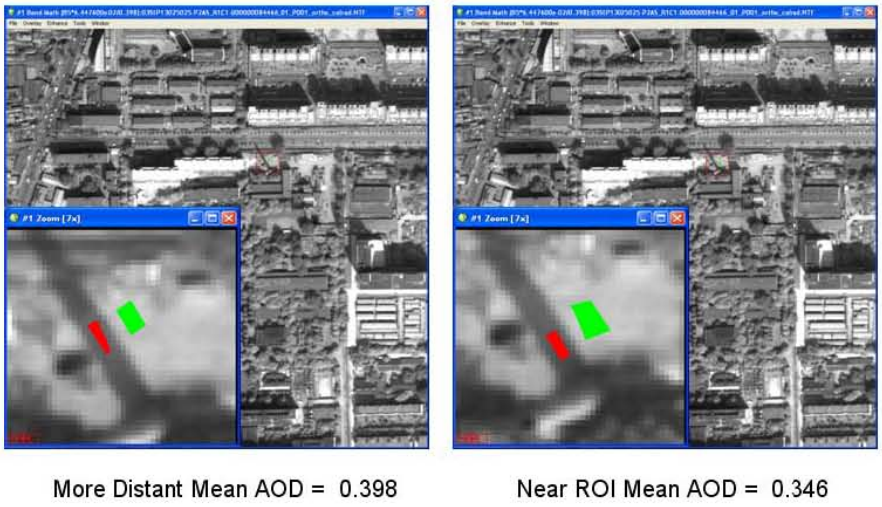

Figure 13. Variation of AOD retrieval within same shadow. More distant AOD of 0.398 and nearer AOD of 0.346.

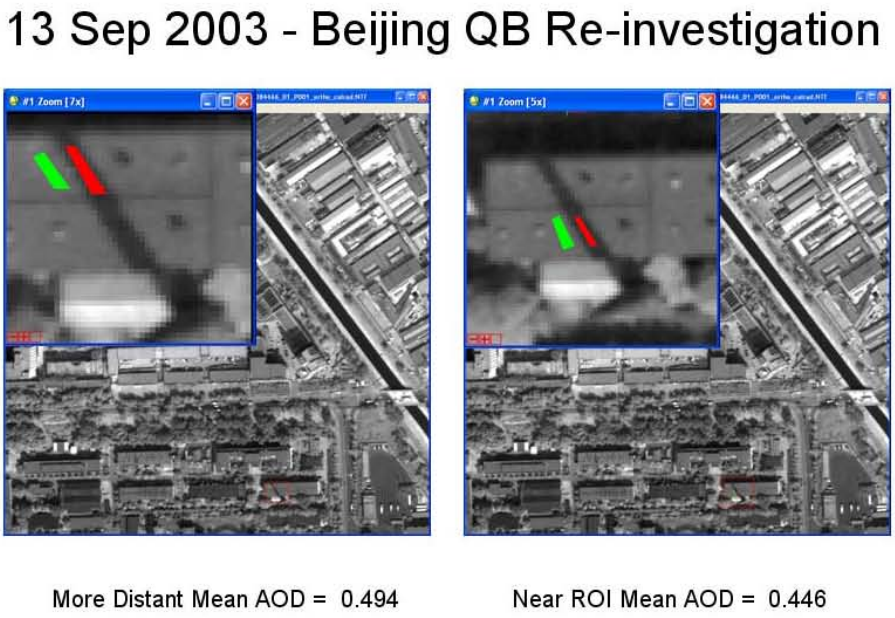

Figure 14. Variation of AOD retrieval within same shadow. More distant AOD of 0.494 and nearer AOD of 0.446.

Another finding of the re-investigation was that the Beijing AERONET station was not in the scene for this image. The AERONET station used to provide ground truth for this case is approximately 3 km to the southeast of the lower right of this image. Evans examined the spatial displacement of his ROIs and AOD values, but did not show a spatial relationship in his data. One theory to explain this lack of spatial variation is the significant low bias resulting from celestial blocking in many of his ROIs. It is quite possible that part of the low bias error attributed to the AOD retrievals may be due to spatial variations in the aerosol between the AERONET station and the ROI locations. Another possible explanation in this variation is the presence of specular reflection in the shaded regions due to variations in surface composition such as observable contrast in the street asphalt. Figure 15 shows AOD retrieval variation within a small section of the Beijing scene.

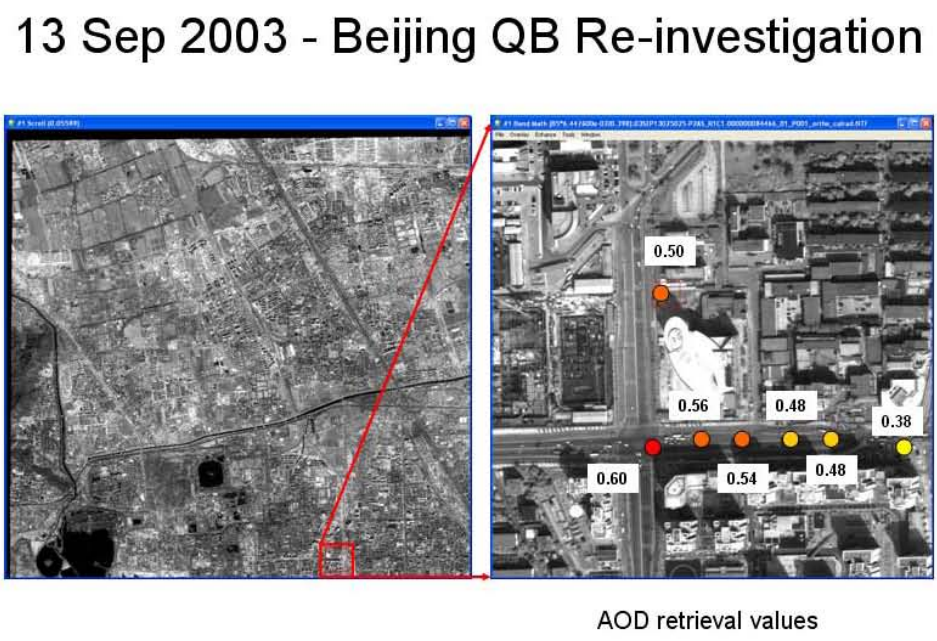

Figure 15. AOD retrieval variation in the Sep 13, 2003, QuickBird image of Beijing China. AOD values varied from 0.38 to 0.60 within a small section of the scene.

ROIs in the scene have asphalt backgrounds and use the outermost corner region of a building shadow. The buildings appear to be similar in size and shape and should have a similar celestial blocking effect. However, within the distance of one city block,

the AOD ranges from 0.6 to 0.38. There is no visible change in the aerosol concentration over this small region. Specular reflection from the background surface is the only plausible explanation for this large variation in AOD retrieval.

3. Findings

Upon re-examination of the image used by Evans (2007), several potential sources of error become evident. ROI selection, specifically the ROI selection within the shaded region has the potential to make a significant difference in the AOD retrieval. Variations in the aerosol concentration may contribute to the AOD error, especially when the AERONET station is not is the scene and AOD retrievals cannot be made very near the observation. Specular reflection may also play a role in AOD variation, breaking the required assumption of a lambertian surface required by the Shadow Method.

VI. QUICKBIRD / WORLDVIEW-1 COMPARISON

A. OVERVIEW

This portion of the study was intended to determine if a spectral response or sensor calibration error in the QuickBird panchromatic sensor may be a factor in the AOD low bias error. The influence of water vapor was also investigated.

1. Case Study Selection

The first factor in determining case study locations was the availability of *in-situ* AOD observation data. The AERONET mapping and location feature on the NASA's AERONET site (http://aeronet.gsfc.nasa.gov/) was used to find stations with a period of record matching that of the WordlView1 satellite, starting in September 2007 (WV1 launch date) to October 2008 (time study conducted). Over 80 stations were identified with data available in September 2007 and approximately 40 stations had data available in October 2008. Regions with the most matching AERONET stations were used to start the search for matching satellite imagery.

The DigitalGlobe ImageFinder web application was used to discover and locate imagery pairs collected over identical or nearby ground locations. Based on the launch date of the WorldView1 satellite a period of 14 months was reviewed. Regions with active AERONET stations during the period of interest were used to start the search. The ImageFinder application provides a filtering feature to search by earliest and latest acquisition date, maximum cloud cover, maximum nadir angle, minimum sun elevation angle, and imaging sensor. The ImageFinder graphic display also shows the coverage area for each collection when the viewing area is zoomed to approximately 1000 km. Five case studies were identified with overlapping or close proximity image collections for both QuickBird and WorldView1.

2. Imagery Processing and Calibration

Images were processed in basically the same methods as outlined by Vincent (2006) and Evans (2007). A significant issue was discovered during the processing of the

archived QuickBird and WorldView1 imagery data. The orthorectification step for the WorldView1 images often required 4-5 days of processing time when run on the available Dell Xenon 3.06 GHz PC (2 GB RAM, 110 GB disk space). This time constraint proved to be unworkable due to network interruptions and planned forced updates from the centralized PC management activity at Naval Postgraduate School (NPS) which would often interrupt the software during the processing period. A LINUX / UNIX version of ENVI 4.5 was installed on 4 processor LINUX based Dell workstations (2GB RAM) and the average orthorectification period was reduced to 2-3 days. This processing period was also deemed to long for eventual transition of the Shadow Method into real time use, so a study was performed to determine the necessity of the orthorectification step.

B. ORTHORECTIFICATION INVESTIGATION

Two location cases were selected in which overlapping QuickBird and WorldView1 images were present. The first image set was collected over Osaka, Japan, on May 17, 2008. The second image set was collected over Cape Verde on January 23, 2008. Both image sets were first orthorectified, then calibrated to TOA radiance as previously outlined. A second control set of the images for each location were *not* orthorectified and only the calibration to TOA radiance step was performed. AOD retrievals were performed on both pairs of imagery using as close to identical ROIs as possible. Identical ROIs are used for the orthorectified and non-orthorectified images for each sensor. Exact ROIs could not be used on both QuickBird and WorldView1 images due to file size and dimension associations in the ENVI software.

1. Osaka, Japan, Case

Figure 16 provides the WorldView1 comparison plot between AOD retrievals from orthorectified and non-orthorectified images of the same scene. Figure 17 provides the QuickBird comparison plot between AOD retrievals from orthorectified and non-orthorectified images of the same scene. AOD retrievals for both panchromatic sensors

show very little variation between the orthorectified and non-orthorectified images. AOD values range from approximately 0.2 to 0.4 for both sensors, with ROI plots falling on or near the 1 to 1 variance line.

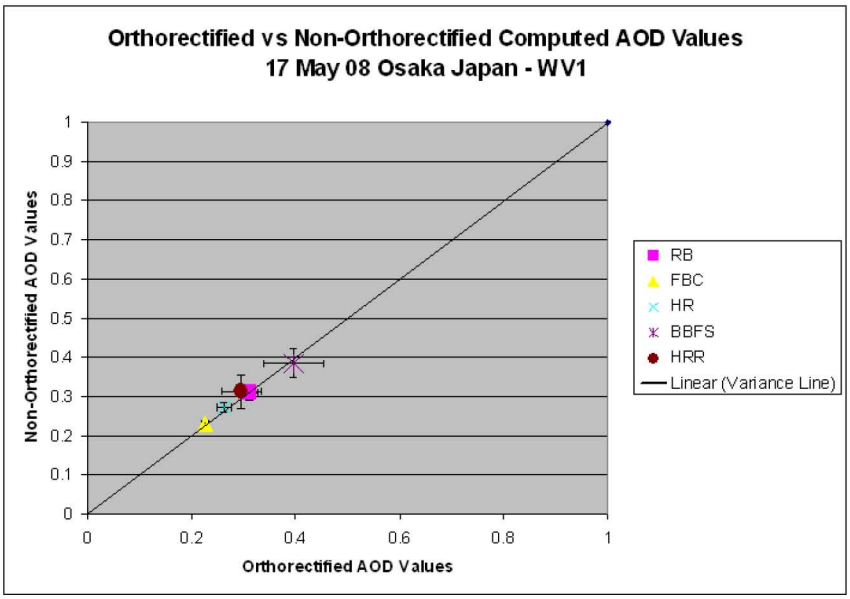

Figure 16. Comparison of AOD results for selected ROIs from orthorectified and non-orthorectified WorldView1 images of Osaka, Japan, on May 17, 2008. Error bars represent one standard deviation.

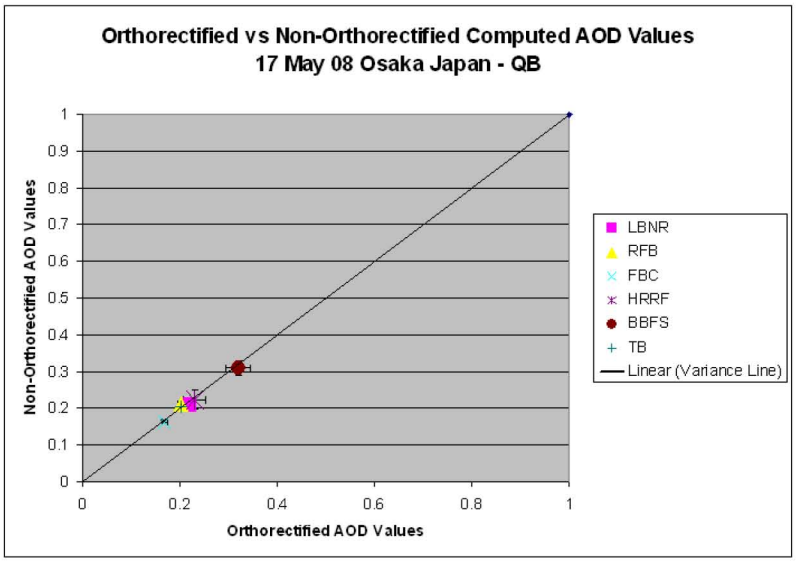

Figure 17. Comparison of AOD results for selected ROIs from orthorectified and non-orthorectified QuickBird images of Osaka, Japan, on May 17, 2008. Error bars represent one standard deviation.

2. Cape Verde Case

Figure 18 provides the WorldView1 comparison plot between AOD retrievals from orthorectified and non-orthorectified images of the same scene. Figure 19 provides the QuickBird comparison plot between AOD retrievals from orthorectified and non-orthorectified images of the same scene. AOD retrievals for both panchromatic sensors show some slight variation between the orthorectified and non-orthorectified images. AOD values range from approximately -0.015 to 0.03 for both sensors. The variation seen in these two images is assumed to be due to the very low AOD values, well below the lower limit for the Shadow Method of 0.1. ROI plots generally fall on or near the 1 to 1 variance line.

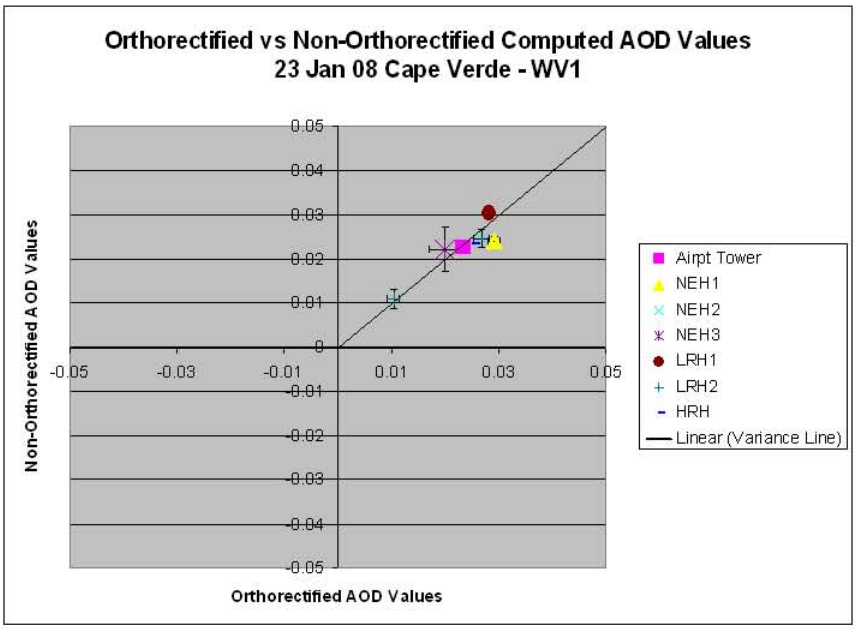

Figure 18. Comparison of AOD results for selected ROIs from orthorectified and non-orthorectified WorldView1 images of Cape Verde on Jan 23, 2008 (AOD < 0.1). Error bars represent one standard deviation.

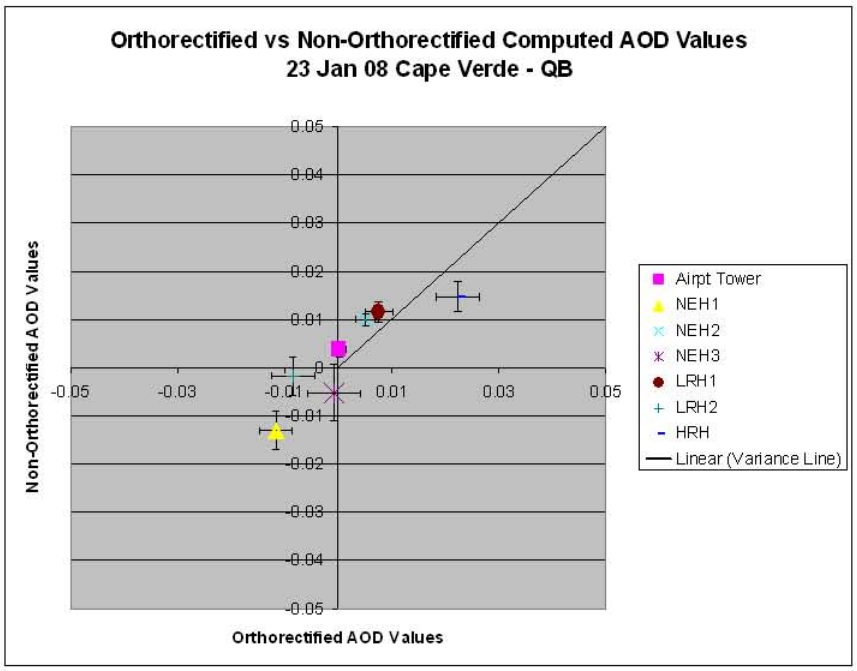

Figure 19. Comparison of AOD results for selected ROIs from orthorectified and non-orthorectified QuickBird images of Cape Verde on Jan 23, 2008 (AOD < 0.1). Error bars represent one standard deviation.

3. Findings

AOD retrievals in the Osaka case for both QuickBird and WorldView1 show each ROI falling on or very near the 1 to 1 variance line well within one standard deviation. The slight difference between the two sensors is due to the manual drawing of ROIs for each separate image. The Cape Verde case shows slightly more variation than the Osaka case due to the very low AOD values present (below 0.1 minimum). Negative AOD values result from the step in the AOD retrieval calculation in which molecular Rayleigh scattering is subtracted from the second iteration of total optical depth as described by Vincent (2006) in the Shadow Method theoretical development. Cape Verde AOD retrievals are nearly all within one standard deviation of the linear variance line.

Based on these results, the orthorectification step was not performed on all subsequent image cases and is not believed to significantly impact AOD retrieval values. If the Shadow Method is used in an operational capacity, the time required for orthorectification of each image would likely prove to be a limiting factor for near real-

time AOD calculations. It is recommended that the orthorectification step in imagery processing be discontinued for operational implementation of the Shadow Method.

C. MOLECULAR RAYLEIGH SCATTERING ANALYSIS

An analysis of molecular Rayleigh scattering was performed to better characterize the potential impact on AOD retrievals. Equations (11) and (12) were used to determine the effect of modifying the initial assumptions used in the calculation of molecular Rayleigh scattering. Sensitivity analysis was performed to examine the potential error resulting from the assumptions of constant atmospheric pressure (1013.25 hPa) and constant station height of zero meters. Plots were generated for both QuickBird and WorldView1 panchromatic channel center effective wavelength (CEW). Station height was varied from zero to 10,000 meters and atmospheric pressure was varied from 900 to 1030 hPa. Figures 20 to 23 show the plots for both panchromatic sensors.

The molecular Rayleigh scattering correction was found to vary from 0.04 to 0.37 for the range in station height range for both sensors. Much less variation was found with changing atmospheric pressure, with molecular Rayleigh scattering correction ranging from approximately 0.038 to 0.045 for the range in atmospheric pressure for both sensors. Based on these results, variation in molecular Rayleigh scattering correction due to atmospheric pressure can effectively be neglected. It is recommended that the molecular Rayleigh scattering correction may need to be adjusted for locations with surface heights above 1000 m in order to properly account for the variation found in this analysis.

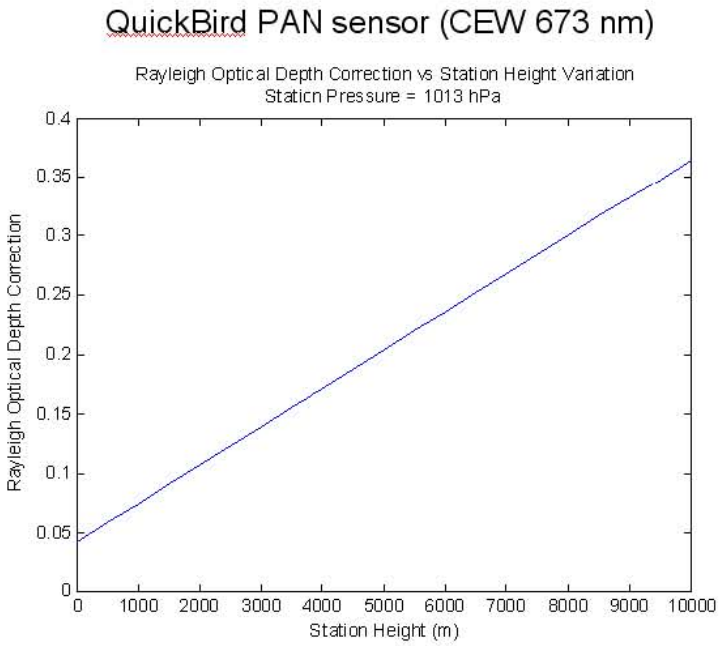

Figure 20. Molecular Rayleigh scattering correction range of values for the QuickBird PAN sensor with variation in station height (m).

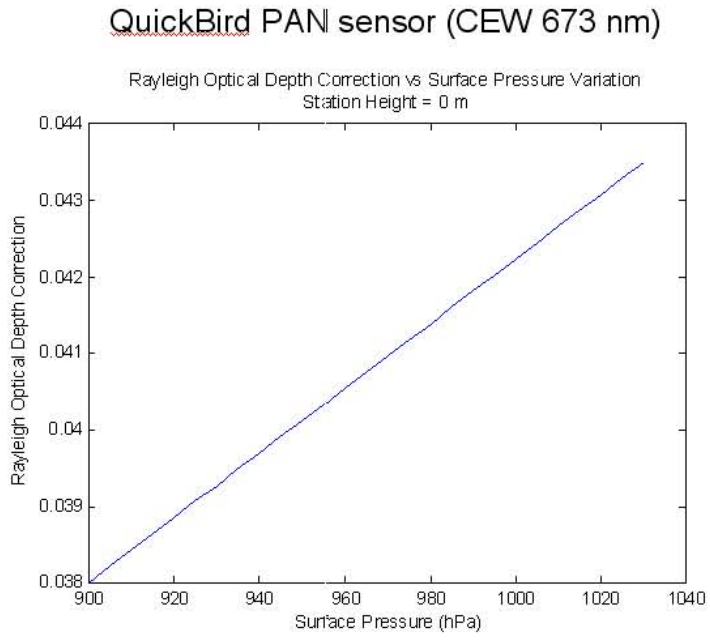

Figure 21. Molecular Rayleigh scattering correction range of values for the QuickBird PAN sensor with variation in surface pressure (hPa).

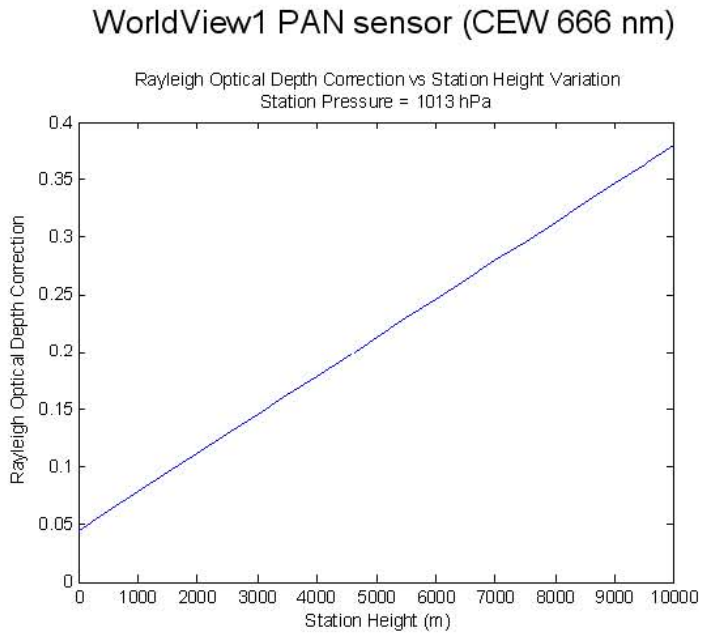

Figure 22. Molecular Rayleigh scattering correction range of values for the WorldView1 PAN sensor with variation in station height (m).

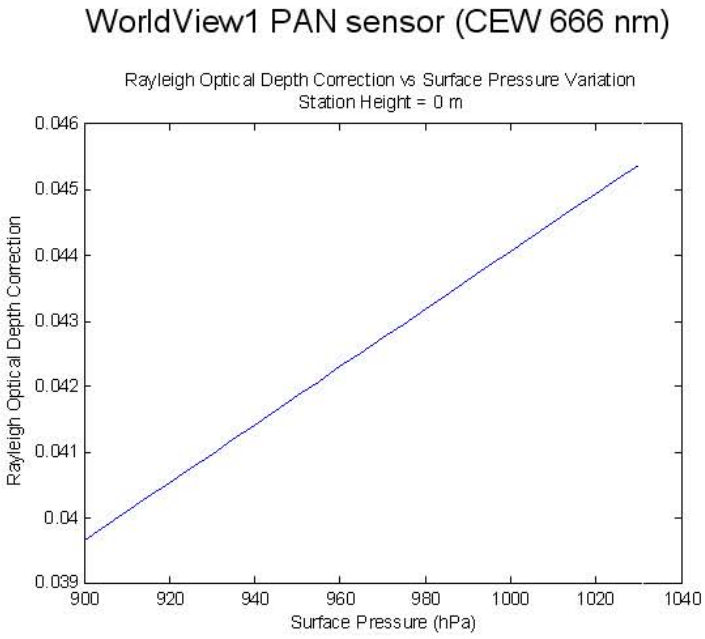

Figure 23. Molecular Rayleigh scattering correction range of values for the WorldView1 PAN sensor with variation in surface pressure.

D. CALIBRATION INVESTIGATION

1. Cape Verde – January 23, 2008, Case

QuickBird and WorldView1 images were collected on January 23, 2008, over San Nicolau Island, Cape Verde. Image collection times were 12:37z for QuickBird and 12:10z for WorldView1. AERONET observations used for ground truth were taken at 12:44z for QuickBird and 11:59z for WorldView1. Integrated AERONET AOD values were 0.33 at 11:59z and 0.31 at 12:44z. The AERONET observation station is located on Sal Island, Cape Verde approximately 90 miles east of San Nicolau Island. Figure 24 shows the location of imagery collection region and the AERONET station. Surface elevations for this case are assumed to be below 100 m, with the AEROENT station height of 60 m. Mean AOD retrievals were 0.018 for WorldView1 and 0.02 for QuickBird. AOD retrievals for the two sensors compared well with each other but varied significantly from the ground truth data. The most likely explanation for this difference is the distance between the AERONET station and the imaged scene (90 miles). It is plausible that the aerosol event during image collection did not extend westward to San Nicolau Island, resulting in much lower AOD retrieval values than those over Sal Island.

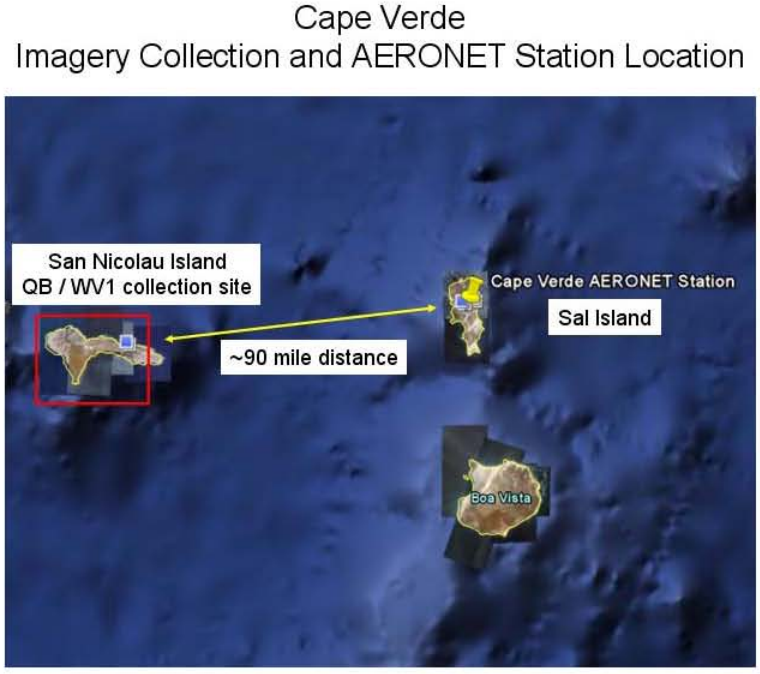

Figure 24. Imagery collection and AERONET station locations – Cape Verde.

2. Dakar, Sengal – May 11, 2008, Case

QuickBird and WorldView1 images were collected on May 11, 2008, over the Dakar peninsula. Image collection times were 12:02z for QuickBird and 11:53z for WorldView1. AERONET observations used for ground truth were taken at 12:05z for QuickBird and 11:50z for WorldView1. Integrated AERONET AOD values were 0.36 for both collection times. Images from both sensors overlapped well allowing for nearly identical ROIs to be used for each image. The AERONET station is located approximately 40 miles to southeast of the imaged area. Figure 25 shows the location of imagery collection region and the AERONET station. Surface elevations for this case are near sea level, with the AERONET station height of zero meters. Mean AOD retrieval was 0.33 for WorldView1 and 0.31 for QuickBird. AOD retrievals between the sensors matched very well, but were lower than the ground truth AOD. The spatial variance between the AERONET station and image collection sites may explain this difference. The AERONET station is located nearer to the inland aerosol source region and may be experiencing elevated aerosol levels compared to the Dakar peninsula.

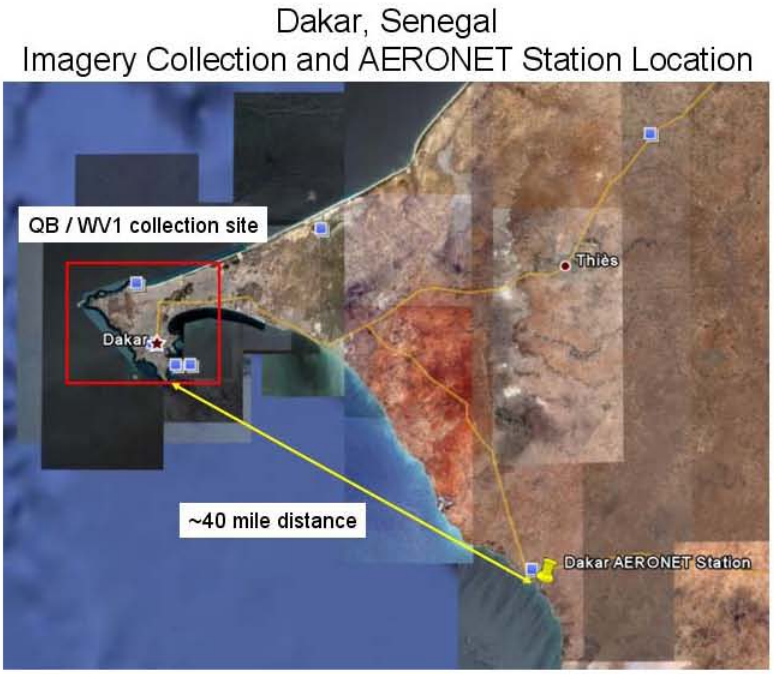

Figure 25. Imagery collection and AERONET station locations – Dakar, Senegal.

3. Kanpur, India – June 24, 2008, Case

QuickBird and WorldView1 images were collected on June 24, 2008, in the vicinity of Lucknow, India. Inage collection times were 05:11z for WorldView1 and 05:35z for QuickBird. No AERONET data was available at the time the image pairs were collected. AERONET observations used for ground truth were taken at 02:14z, June 23, 2008. This observation was the nearest available to the image collection times providing an estimated ground truth AOD value of 0.85. The AERONET station was located approximately 50 miles to southwest of the image collection area. Figure 26 shows the location of imagery collection region and the AERONET station. Due to large temporal and spatial variation between ground truth observation and image collection times, it was expected that AOD retrievals would vary from ground truth AOD.

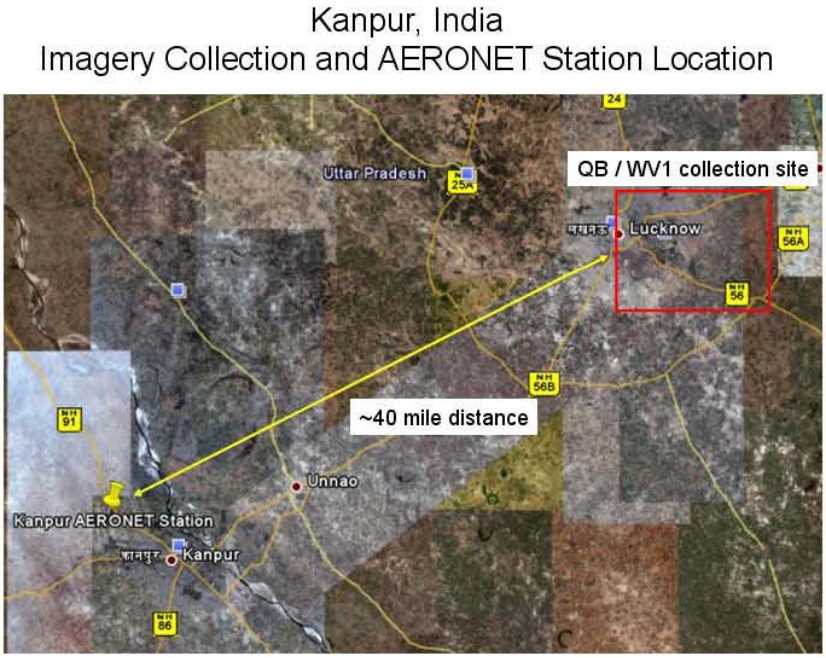

Figure 26. Imagery collection and AERONET station locations – Kanpur, India.

The mean AOD for the WorldView1 image, collected first, was 0.53. The QuickBird image taken 24 minutes later revealed large spatial variation in AOD retrievals. ROIs selected in the southwest region of the image resulted in a mean AOD of 0.69, while ROIs selected in the northeast region of the image resulted in a mean AOD of

0.28. Figure 27 shows the AOD retrieval plots for this case. Obscuration is actually visible in the southwestern region of the image. Based on the AERONET station's location to the southwest of the imaged area and the increasing AOD retrieval values seen in the later QuickBird image, it appears that the aerosol obscuration is advecting from the southwest to the northeast.

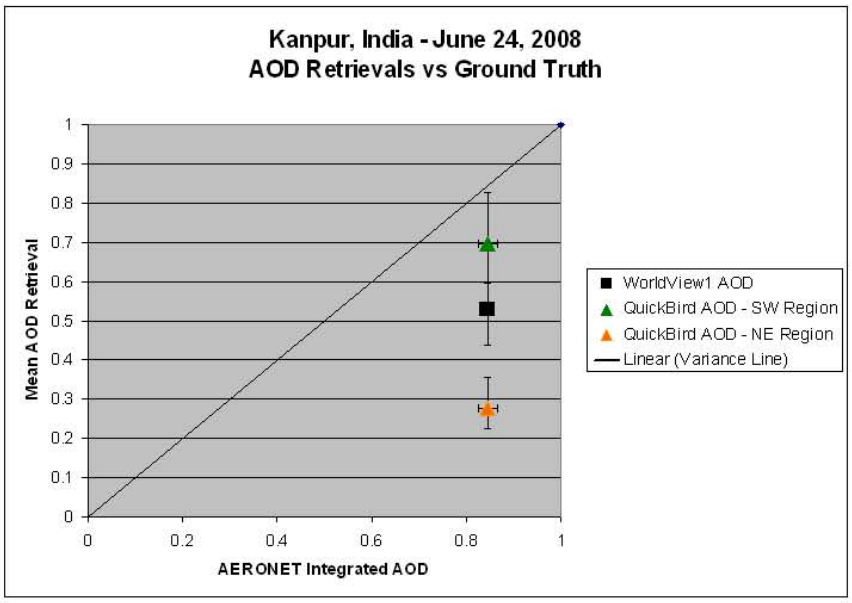

Figure 27. AOD retrievals for Kanpur, June 24, 2008. Error bars show range of AOD retrieval values and AERONET error. Larger AOD values were found in the southwest region of the QuickBird image, while smaller values were found in the northeast region.

4. Osaka, Japan - May 17, 2008, Case

QuickBird and WorldView1 images were collected on May 17, 2008, over Osaka, Japan. Image collection times were 01:43z for WorldView1 and 02:04z for QuickBird. AERONET observations used for ground truth were taken at 01:40z for WorldView1 and 02:25z for QuickBird. Ground truth observations are approximately 45 minutes apart, with integrated AOD values of 0.66 for the WorldView1 image and 0.56 for the QuickBird image. The AERONET station was located inside the imaged area. Figure 28 shows the location of imagery collection region and the AERONET station. Surface elevations for this case are assumed close to the AERONET station height of 50 m.

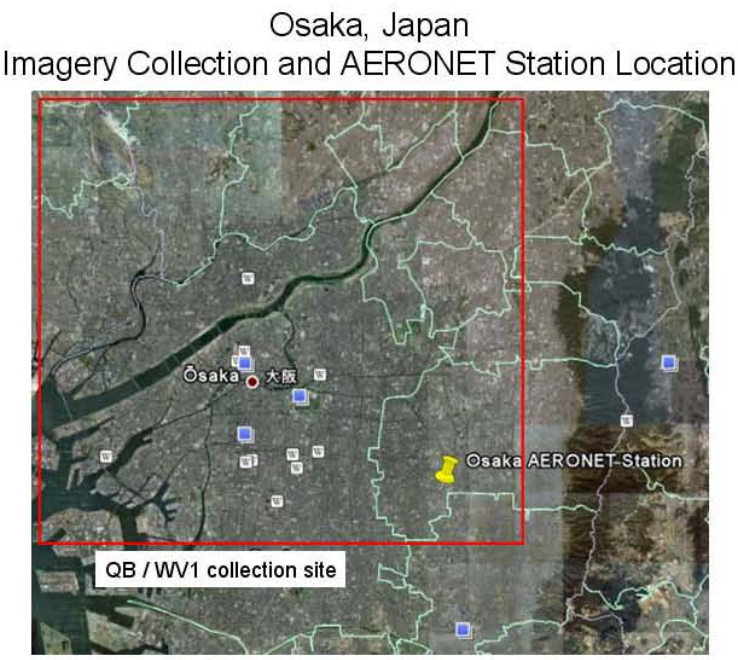

Figure 28. Imagery collection and AERONET station locations – Osaka, Japan.

Both panchromatic images in the Osaka case showed a large amplitude AOD low bias when compared to the ground truth data. Mean AOD retrievals were 0.39 for WorldView1 and 0.27 for QuickBird. Ground truth data was available within three minutes of the WorldView1 image and 20 minutes of the QuickBird data, yet both have an average low bias of 42% (WV1) and 51% (QB) respectively. As with the previous cases, care was taken to avoid celestial blocking of the ROIs. No explanation for this low bias could be determined. Though there was a large low bias in this case, the sensors again appear to provide roughly equal results.

5. Sede Boker, Israel – January 24, 2008, Case

QuickBird and WorldView1 images were collected on January 24, 2008. Images collection times were 08:35z for WorldView1 and 08:51z for QuickBird. Closest AERONET observation to image collection times was 13:19z and the integrated AOD value of 0.08 used as ground truth for both cases. The AERONET station is located approximately 40 miles to the southeast of the imaged region. Figure 29 shows the

location of imagery collection region and the AERONET station. The AERONET station elevation is 400m and the imaged region is assumed to be lower than this station height due to proximity to the coast.

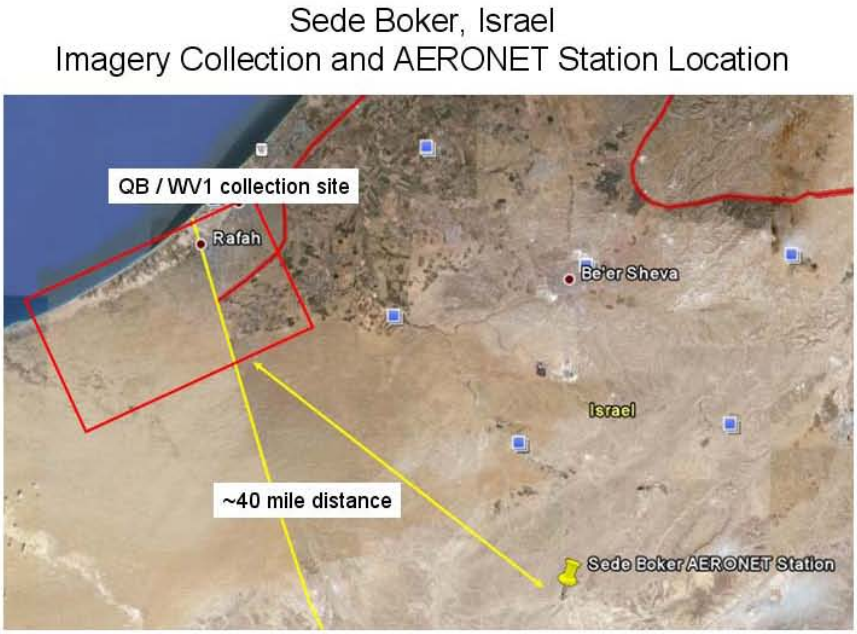

Figure 29. Imagery collection and AERONET station locations – Sede Boker, Israel.

AOD retrievals for both sensors compared very well to each other in spite of a 20 minute period between image collections. Mean AOD values of 0.11 and 0.12 were very close to ground truth observations collected 40 miles away. The aerosol appears to have been homogenous both spatially and temporally over the entire region.

6. Findings

AOD retrievals from overlapping QuickBird and WorldView1 images taken within minutes of each other show comparable results, effectively ruling out a calibration issue with the QuickBird panchromatic sensor. Low bias in the AOD retrievals compared to ground truth is greatest when there is a large temporal gap between the AERONET observation and the image collection time or a large spatial difference in the AERONET observation location and imaged region. Variation between the two sensors is greatest when the collection time interval is longer, allowing for greater variation in the aerosol atmospheric concentration. The two cases with largest mean AOD retrieval difference

had approximately 20 minutes between image collections. Table 7 provides the integrated AERONET ground truth data and AOD retrievals for the ten images used in this sensor calibration study. Figure 30 illustrates the results of the QuickBird / WorldView1 panchromatic sensor comparison for the 5 image pair cases. Overall, the AOD retrievals are very close between the two panchromatic sensors for the cases with nearest image collection times. Based on the results of this analysis, it is determined that there is no apparent source of error in the QuickBird panchromatic sensor calibration.

Table 7. Integrated AERONET ground truth and AOD retrievals for each sensor / image in the calibration study.

Location	Sensor	Ground Truth AOD	Mean AOD Retrieval
Cape Verde 012308	WV1	0.33	0.018
Cape Verde 012308	QB	0.31	0.02
Dakar 051108	WV1	0.36	0.33
Dakar 051108	QB	0.36	0.31
Kanpur 062408	WV1	0.85	0.53
Kanpur 062408	QB	0.85	0.69
Osaka 051708	WV1	0.66	0.39
Osaka 051708	QB	0.56	0.27
Sede Boker 012408	WV1	0.08	0.11
Sede Boker 012408	QB	0.08	0.12

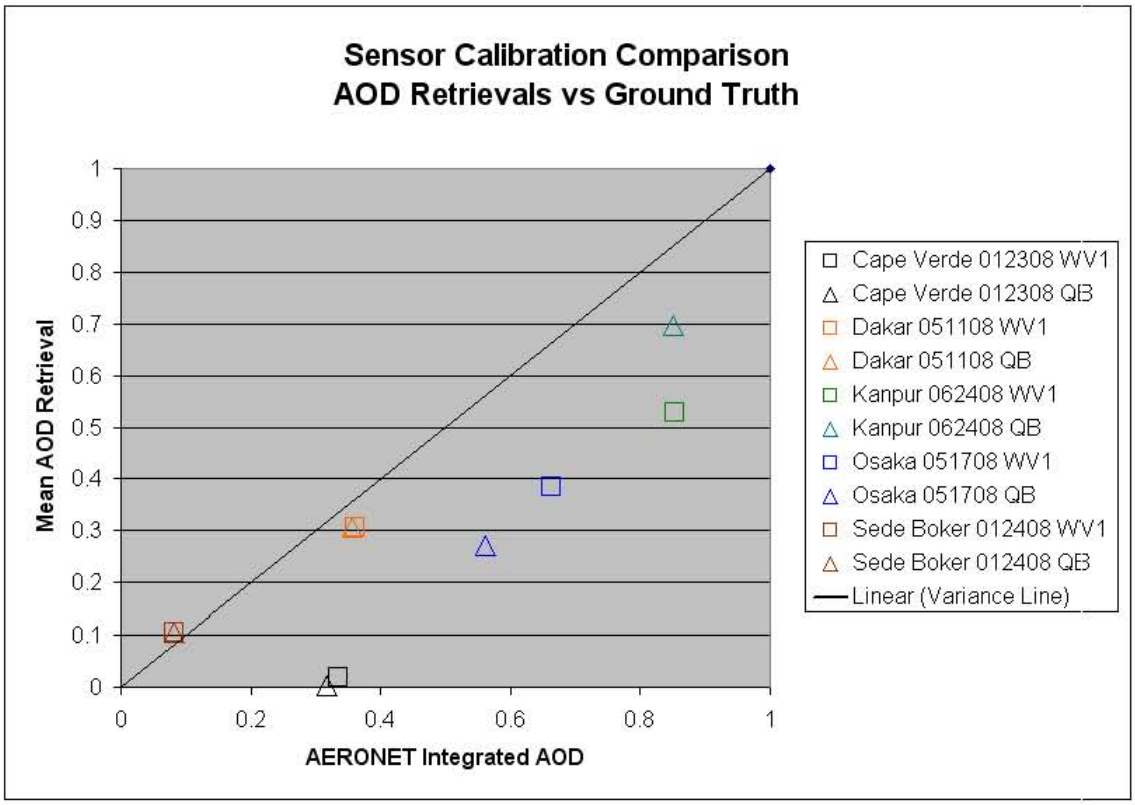

Figure 30. QuickBird / WorldView1 panchromatic sensor comparison of AOD retrievals for co-located image pairs. Best results are seen for image pairs with shortest temporal interval.

E. WATER VAPOR INVESTIGATION

1. High Water Vapor Cases

Five image collections were selected as high water vapor content cases. AERONET observations with water vapor content greater than 2 cm were deemed to be high content cases. All five high water vapor cases were WorldView1 panchromatic images. Water vapor content ranged from 2.2 to 4.4 cm for the five image cases. AOD ground truth values ranged from 0.17 to 0.58. Three cases showed excellent AOD retrieval agreement with ground truth. Two cases had a low bias when compared to ground truth. Table 8 lists the mean AOD retrieval values, ground truth observations and water vapor content for the high water vapor cases. Figure 31 shows the plot of all five high water vapor content cases versus ground truth.

Table 8. Mean AOD retrievals, water vapor content and ground truth AOD observations for the five high water vapor content cases.

Location / Date	Mean AOD Retrieval	Ground Truth AOD	Water Vapor (cm)
Beijing 062108	0.153	0.319	2.2
Cape Verde 051508	0.184	0.173	2.4
Dakar 051108	0.330	0.352	2.3
Dakar 052408	0.492	0.583	2.4
Osaka 081108	0.179	0.183	4.4

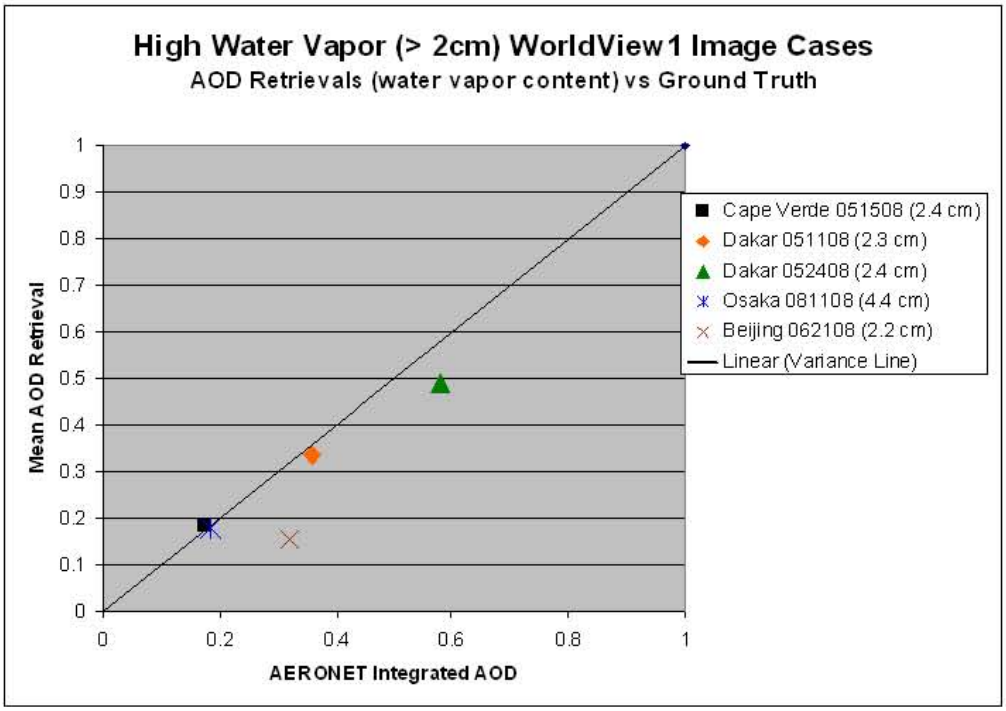

Figure 31. High water vapor content (> 2cm) cases. AOD retrievals vs. ground truth data are plotted. Water vapor content is listed for each case in the legend.

The Beijing case of June 21, 2008, produced an AOD retrieval approximately 50% lower than the ground truth. The AERONET observation station was within the imaged scene and observations are within 9 minutes of the image collection time. No satisfactory explanation could be determined for this large low bias.

The Osaka case of August 11, 2008, had the highest water vapor content of all cases at 4.4 cm. The AOD retrievals in this case matched ground truth data nearly

exactly (within 0.01). Based on these five cases with water vapor greater than 2 cm, water vapor content does not appear to influence AOD retrievals.

2. Low Water Vapor Cases

Five image collections were selected as low water vapor content cases. AERONET observations with water vapor content greater than 1 cm were deemed to be low content cases. Water vapor content ranged from 0.74 to 0.95 cm for the five image cases. AOD ground truth values ranged from 0.08 to 1.29. Four cases showed excellent AOD retrieval agreement with ground truth. The case with the largest overall AOD values had a low bias when compared to ground truth. Table 9 lists the mean AOD retrieval values, ground truth observations and water vapor content for low water vapor cases. Figure 32 shows the plot of all five low water vapor content cases versus ground truth.

Table 9. Mean AOD retrievals, water vapor content and ground truth AOD observations for the five low water vapor content cases

Location / Date	Mean AOD Retrieval	Ground Truth AOD	Water Vapor (cm)
Beijing 032708	0.147	0.152	0.74
Sede Boker 012408	0.106	0.081	0.69
Sede Boker 012408	0.122	0.08	0.69
SolarVillage 041808	1.08	1.29	0.92
SolarVillage 101108	0.168	0.263	0.95

The Solar Village Case of April 18, 2008, had the largest AOD values for either water vapor category. The mean AOD retrieval was within 84% of the ground truth observation. The AERONET observation was taken within 1 minute of the WorldView1 image, but was not located in the image scene. The AERONET station was approximately 40 miles southeast of the imaged location. The spatial variation could explain the slightly different results in AOD retrieval compared to ground truth.

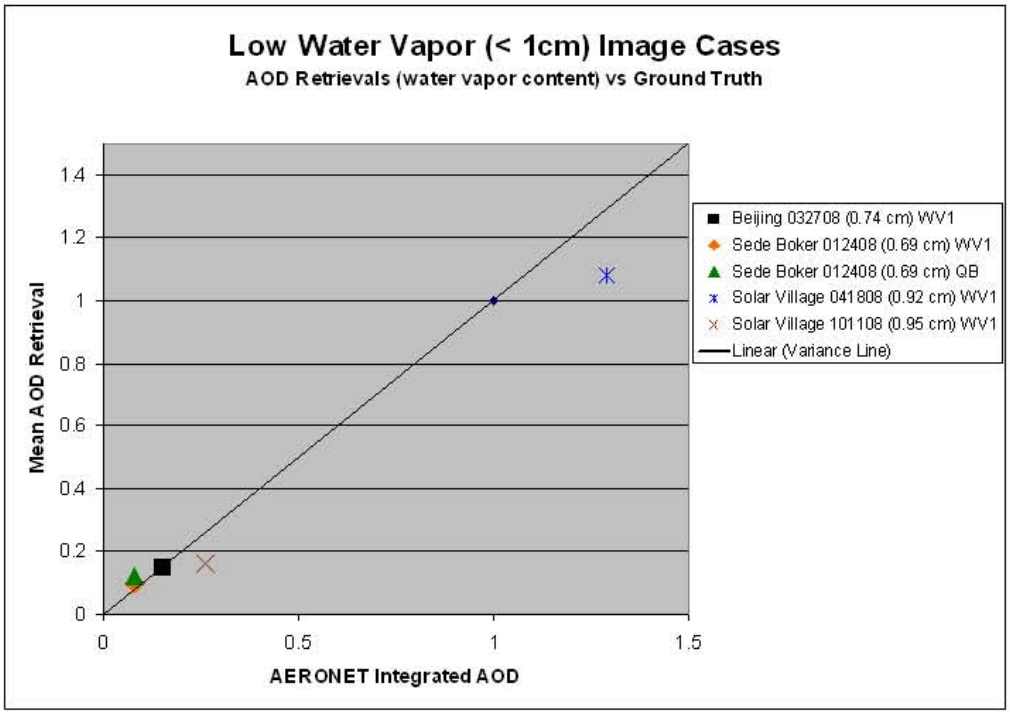

Figure 32. Low water vapor content (< 1 cm) cases. AOD retrievals vs. ground truth data are plotted. Water vapor content is listed for each case in the legend.

Table 10 provides the water vapor content and low bias amplitude for the high and low water vapor content cases. The negative low bias amplitude values reflect a mean AOD retrieval value larger than the ground truth AOD value, or a negative low bias. Figure 33 shows the correlation plot for all ten high and low water vapor cases studied. The correlation coefficient (R^2) for the plot in Figure 33 is only 0.0036, showing no linear correlation between water vapor content and low bias amplitude.

Table 10. Water vapor content (cm) and low bias amplitude for high and low water content cases.

Image Case	Water Vapor Content (cm)	Low Bias Amplitude
Beijing 062108	2.2	0.16
Cape Verde 051508	2.4	-0.011
Dakar 051108	2.3	0.022
Dakar 052408	2.4	0.091
Osaka 081108	4.4	0.004
Beijing 032708	0.74	0.01
Sede Boker 012408	0.69	-0.025
Sede Boker 012408	0.69	-0.042
SolarVillage 041808	0.92	0.21
SolarVillage 101108	0.95	0.098

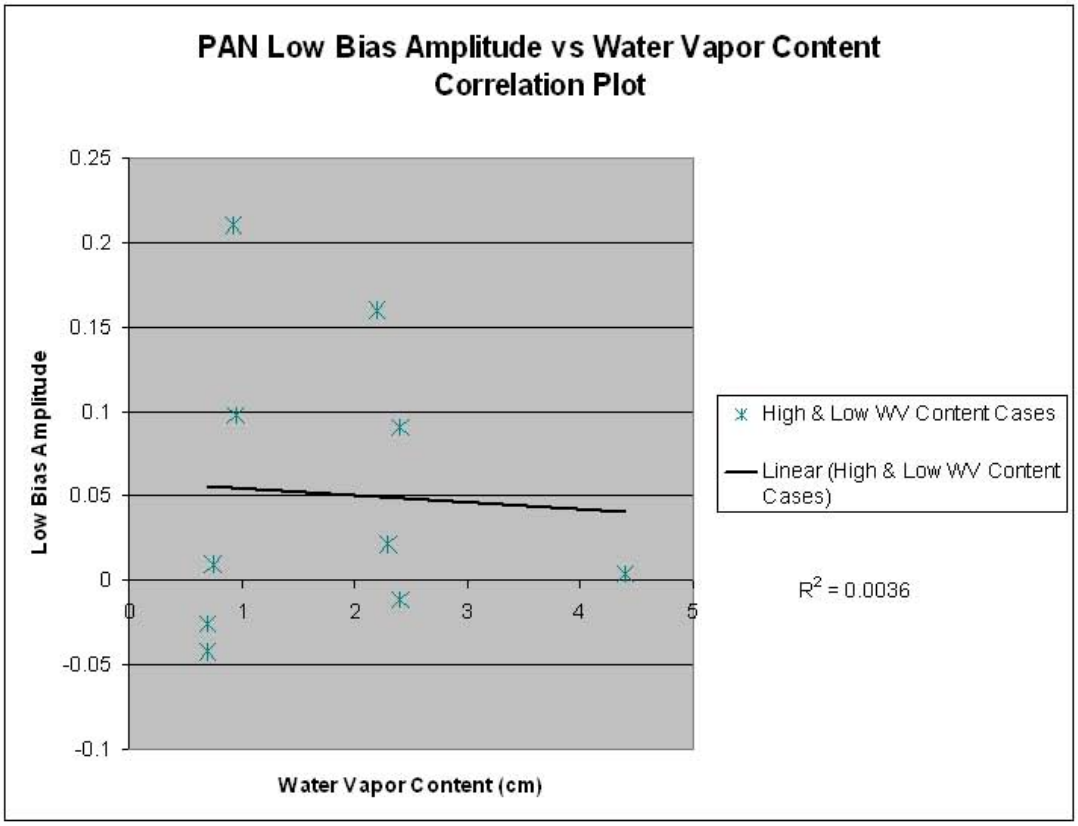

Figure 33. Correlation plot of water vapor content (cm) vs low bias amplitude for the ten high and low water vapor cases.

3. Findings

Panchromatic AOD retrieval errors do not appear to correlate with atmospheric water vapor content. The largest variation between AOD retrieval and ground truth do not occur in the cases with highest water vapor content. With the exception of the June 21, 2008, Beijing case, most errors in retrieved AOD could be explained by variation in the AOD concentration due to temporal or spatial differences between ground truth observation and image collection time.

THIS PAGE INTENTIONALLY LEFT BLANK

VII. CONCLUSION

A. CONCLUSIONS

1. Previous Case Studies Investigation

Time Delay Integral and absolute calibration factor variation were investigated as potential causes for the panchromatic channel low bias error seen in previous research on the Shadow Method by Vincent (2006) and Evans (2007). Only one previous image collection case was found to have a TDI and absolute calibration factor which differed from the values used by Vincent and Evans. There were no differences in TDI or absolute calibration factor for the cases with the largest low bias error. Atmospheric water vapor content did not correlate with the low bias signal seen in previous research cases. The largest source of error seen in previous cases is most likely due to a combination of factors. Spatial differences between ground truth observation sites and image collection locations often results in AOD retrieval differences due to variation in the atmospheric aerosol concentration. Region of interest (ROI) selection can have a large impact on AOD retrieval values due to the effects of celestial blocking from large shadow generators. The re-investigation of Evans' Beijing image using more stringent ROI selection criteria resulted in an increase in mean AOD retrieval from 0.30 to 0.44, with a ground truth value of 0.55

2. QuickBird / WorldView1 Comparison

Orthorectification of satellite imagery prior to application of the Shadow Method was shown to have no significant impact on AOD retrievals. It is recommended that the orthorectification step not be performed due to the long processing time required to complete this step. The molecular Rayleigh scattering correction was found to vary with station height. It is recommended that surface height influence be included in the Rayleigh correction calculation for those cases with surface elevations more than 1000 meters. The comparison between co-collected QuickBird and WorldView1 images did not reveal a significant difference in AOD retrievals between the two panchromatic sensors. This finding effectively rules out the theory that sensor calibration error may be

responsible for the low bias error. Overall results with the WorldView1 panchromatic sensor overall were consistent with previous results using the QuickBird panchromatic sensor. Water vapor content effects on AOD retrieval values were examined and found to have no apparent influence.

Based on the findings in this study the largest source of error in the Shadow Method appears to be the selection of shadow generators and detailed placement of the ROI shaded / unshaded regions. Best results are obtained when using shadows which are longer than they are wide. Shadow generators such as smokestacks, water towers and other tall, narrow objects effectively reduce the celestial blocking effect. These shadows allow more reflected radiance from the suspended aerosol to reach the shaded region, reducing the low bias and providing more accurate AOD retrievals. The only limit to these narrow shadows is the necessity to have 2-3 pixels within the shadow which are not influenced by edge effects in what Dombrock (2006) referred to as the transition zone. This translates to a minimum shadow generator width of about 1-1.5 meters for the WorldView1 and QuickBird panchromatic channels and about 5-7 meters for the multispectral channels.

B. RECOMMENDATIONS FOR FUTURE RESEARCH

Commercial satellite imagery should be collected at controlled test sites where ground truth AOD observations can be collected coincident with the imagery and surface reflectance can be characterized more accurately. A controlled, reconfigurable shadow generator should be used to compare regions of interest generated using multi-spectral and panchromatic channels. The comparison may reveal radiance characterization differences resulting from the large spatial resolution disparity between the two the sensor classes.

Efforts to further reduce the time required to apply the Shadow Method should be pursued. This method will be an effective tool for estimating AOD in denied or remote areas even with the current errors seen in recent research. The sensitive nature of shadow selection and ROI composition may make automation a difficult task. Streamlining the

process to use predetermined target locations based on predicted shadows and satellite orbital characteristics, as suggested by Dombrock (2007), might be the best approach to move this method into operational use.

Additional research should be conducted using the forthcoming WorldView2 satellite from DigitalGlobe. This satellite will combine a panchromatic sensor with an expanded number of multispectral channels compared to QuickBird. Additional multispectral channels will include a blue band centered at 425 nm, a yellow band centered at 605 nm, a red edge band at 725 nm and a longer infrared band at 950 nm (Digital Globe, 2008). These additional channels may help to resolve those cases in which the low bias cannot be definitively explained.

THIS PAGE INTENTIONALLY LEFT BLANK

LIST OF REFERENCES

Brown, B. A., 2002: Aerosol optical depth retrieval by NPS model modified for SeaWIFS. M.S. thesis, Dept. of Meteorology, Naval Postgraduate School, Monterey, CA.

Brown, B. B., 1997: Remote measurement of aerosol optical properties using NOAA POES AVHRR and GOES imagery during TARFOX. M.S. thesis, Dept. of Meteorology, Naval Postgraduate School, Monterey, CA.

DigitalGlobe, cited July 2008: QuickBird Specifications. [Available online at http://www.digitalglobe.com/index.php/85/QuickBird].

DigitalGlobe, cited July 2008: WorldView-1 Specifications. [Available online at http://www.digitalglobe.com/index.php/86/WorldView-1.]

DigitalGlobe, cited July 2008: WorldView-2 Specifications. [Available online at http://www.digitalglobe.com/index.php/88/WorldView-2.]

Dombrock, R., 2007: Automating shadow method for AOD retrieval. M.S. thesis, Dept. of Meteorology, Naval Postgraduate School, Monterey, CA.

Durkee, P., K. Nielsen, N. Vincent, Z. Jianglong, J. Reid, 2008: Multi-Spectral Aerosol Properties from High-Resolution Satellite Imagery. MEPIC Conference, Apr 2008.

Evans, J. R., 2007: A verification of optical depth retrievals from high resolution satellite imagery. M.S. thesis, Dept. of Meteorology, Naval Postgraduate School, Monterey, CA.

Garmin Ltd, cited Sep 2008: Discontinued Models. [Available online at http://www.garmin.com/garmin/cms/site/us/.]

Green, R. O., M. L. Eastwood, C. M. Satrure, 1998: Imaging spectroscopy and the Airborne Visible/Infrared Imaging Spectrometer (AVIRIS). *Remote Sensing of the Environment*, **65**, 227-248.

Goddard Space Flight Center (GSFC), cited Aug 2008: Aerosol robotic network (AERONET) mission. [Available online at http://aeronet.gsfc.nasa.gov/.]

Holben, B. N., T. F. Eck, I. Slutsker, D. Tanre, J. P. Buis, A. Setzer, E. Vermote, J. A. Reagan, Y. J. Kaufman, T. Nakajima, F. Lavenu, I. Jankowski, and A. Smirnov, 1998: AERONET – A federated instrument network and data archive for aerosol characterization. *Remote Sensing of the Environment*, **66**, 1-16.

Hsu, N C., S. C. Tsay, M. D. King, and J. R. Herman, 2004: Aerosol properties over bright-reflecting source regions. *IEEE Trans. Geosci. Remote Sens.*, **42**, 557-569.

Jet Propulsion Lab (JPL) California Institute of Technology (CIT), cited Nov 2008: AVIRIS Concept. [Available on-line at http://aviris.jpl.nasa.gov/html/aviris.overview.html.]

Kaufman, Y. J., and J. H. Joseph, 1982: Determination of surface albedos and aerosol extinction characteristics from satellite imagery. *J. Geophys.Res.*, **87**, 1287-1299.

Kaufman, Y. J., and C. Sendra, 1988: Algorithm for automatic atmospheric corrections to visible and near-IR satellite imagery. *Int. J. Remote Sens.*, **9**, 1357-1381.

Krause, K., 2008: Personal Communication. DigitalGlobe, Inc.

Krause, K., 2003: Radiance Covnersion of QuickBird Data. DigitalGlobe, Inc. Tech. Note RS_TN_radiometric_radiance_4002, 4 pp. Cited Feb 2009 [Available on-line at http://www.pci.on.ca/discuss-archive/pdf00001.pdf.]

Kuciauskas, A. P., 2002: Aerosol optical depth analysis with NOAA, GOES, and POES in the Western Atlantic. M.S. thesis, Dept. of Meteorology , Naval Postgraduate School, Monterey, CA.

Martin, J. S., 2004: Aerosol optical depth model assessment with high resolution multiple angle sensors. M.S. thesis, Dept. of Meteorology, Naval Postgraduate School, Monterey, CA.

Martonchik, J. V., D. J. Diner, R. Kahn, and B. Gaitley, 2004: Comparison of MISR and AERONET aerosol optical depths over desert sites. *J. Geophys. Res.*, **31**, L16102, 1-4.

NASA Earth Observatory, cited July 2008: Image of the Day [Available on-line at http://earthobservatory.nasa.gov/IOTD/].

Odell, A. P. and J. A. Weinman, 1975: The effect of atmospheric haze on images of the earth's surface. *J. Geophys. Res.*, **80**, 5035-5040.

Russell, P. B., J. M. Livingston, E. G. Dutton, 1993: Pinatubo and pre-Pinatubo optical depth spectra: Mauna Loa measurements, comparisons, inferred particle size distributions, radiative effects, and relationship to lidar data. *J. Geophys. Res.*, **98**, 22969-22985.

Solar Light Company Inc., cited Sep 2008: Product and Services, Aerosols [Available on-line at http://www.solar.com/].

Tanre, D., M. Herman, and P. Y. Deschamps, 1981: Influence of the background contribution upon space measurements of ground reflectance. *Appl. Opt.*, **20**, 3676-3684.

Veefkind, J. P., G. de Leeuw, P. Stammes, and R. B. A. Koelemeijer, 1998: Regional distribution of aerosol over land derived from ATSR-2 and GOME. *Rem. Sens. Env.*, **74**, 377-386.

Vincent, D. A., 2006: Aerosol optical depth retrievals from high-resolution commercial satellite imagery over areas of high surface reflectance. Dissertation, Naval Postgraduate School, Monterey, CA.

Wehrli, C., 1985: *Extraterrestrial Solar Spectrum - Publ. 615*. Physical Meterological Observatory and World Radiation Center, Davos Dorf, Switzerland.

THIS PAGE INTENTIONALLY LEFT BLANK

INITIAL DISTRIBUTION LIST

1. Defense Technical Information Center
   Ft. Belvoir, Virginia

2. Dudley Knox Library
   Naval Postgraduate School
   Monterey, California